Front. Phys., 2014, 9(5): 539–570
DOI 10.1007/s11467-014-0448-7

REVIEW ARTICLE

Pseudogap phenomena in ultracold atomic Fermi gases

Qijin Chen† **and Jibiao Wang**

Department of Physics and Zhejiang Institute of Modern Physics, Zhejiang University, Hangzhou 310027, China

Corresponding author. E-mail: †*qchen@zju.edu.cn*

Received September 7, 2014; accepted September 14, 2014

The pairing and superfluid phenomena in a two-component ultracold atomic Fermi gas is an analogue of Cooper pairing and superconductivity in an electron system, in particular, the high T_c superconductors. Owing to the various tunable parameters that have been made accessible experimentally in recent years, atomic Fermi gases can be explored as a prototype or quantum simulator of superconductors. It is hoped that, utilizing such an analogy, the study of atomic Fermi gases may shed light to the mysteries of high T_c superconductivity. One obstacle to the ultimate understanding of high T_c superconductivity, from day one of its discovery, is the anomalous yet widespread pseudogap phenomena, for which a consensus is yet to be reached within the physics community, after over 27 years of intensive research efforts. In this article, we shall review the progress in the study of pseudogap phenomena in atomic Fermi gases in terms of both theoretical understanding and experimental observations. We show that there is strong, unambiguous evidence for the existence of a pseudogap in strongly interacting Fermi gases. In this context, we shall present a pairing fluctuation theory of the pseudogap physics and show that it is indeed a strong candidate theory for high T_c superconductivity.

Keywords pseudogap, pairing fluctuation theory, atomic Fermi gases, BCS–BEC crossover, high T_c superconductivity

PACS numbers 03.75.Ss, 03.75.Hh, 67.85.Pq, 74.25.Dw

Contents

1 Introduction

Study of atomic Fermi gases, especially the pairing and superfluid phenomena, has become a major field

in physics research over the last decade [1, 2]. Intrinsically a many-body system, atomic Fermi gases have attracted physicists from both condensed matter and atomic, molecular and optics (AMO) communities, as well as from other communities, e.g., nuclear and particle physics and astrophysics. Even superstring theorists have now found it a play ground for the ingenious idea of the AdS/CFT correspondence [3–6]. This is primarily due to the fact that many tunable parameters have been made accessible experimentally for atomic Fermi gases, including temperature, pairing interaction strength, pairing symmetry, population imbalance, mass imbalance, geometric aspect ratio of the trap, optical lattices, and dimensionality, etc., as well as extra degrees of freedom such as spin-orbit coupling and synthetic gauge fields, which make atomic gases a suitable system for quantum simulation and quantum engineering of existing and previously unknown systems, and have thus provided a great opportunity for studying many exotic quantum phenomena.

In terms of superfluidity, atomic Fermi gases can be thought of as the charge neutral counterpart of superconductors, which have been an important subject in contemporary condensed matter physics. In particular, high T_c superconductivity has been a great challenge since its discovery a quarter century ago. With tunable interactions, it is strongly hoped that one may learn about the notoriously difficult problem of high T_c superconductivity via studying atomic Fermi gases.

At the heart of the high T_c problem is the widespread anomalous normal state gap [7] in the single particle excitation spectrum, which has been referred to as the *pseudogap*, and has emerged since the discovery of high T_c superconductors. It is essential to understand the pseudogap phenomena in order to reach a consensus on the mechanism of high T_c superconductivity. Due to the analogy between superfluidity and superconductivity, it is expected that study of the pairing and superfluid phenomena in ultracold Fermi gases may eventually shed light on the pseudogap physics and thus the mechanism of high T_c superconductivity.

The first and most widely explored parameter in ultracold atomic Fermi gases is the pairing interaction strength. Using an s-wave Feshbach resonance, one can tune the effective pairing strength from the weak coupling limit of Bardeen–Cooper–Schrieffer (BCS) superfluidity [8] all the way through the strong coupling limit of Bose–Einstein condensation (BEC) [9–12]. In this way, the theoretical idea of BCS–BEC crossover, which was first proposed by Eagles [13] and Leggett [14] at zero temperature T and then extended to finite T by Nozières and Schmitt-Rink [15] and many others [16–36], can be realized and studied systematically in experiment.

There have been a few milestones in experimental studies of the superfluidity and BCS–BEC crossover of ultracold Fermi gases. Degenerate Fermi gases was achieved a few years [37] after the experimental realization of BEC of dilute gases of bosonic alkali atoms [38–41], such as ^{23}Na, ^{87}Rb, and ^{7}Li. BEC of diatomic molecules on the BEC side of a Feshbach resonance was first reported in 2003 in Fermi gases of ^{40}K and of ^{6}Li [42–44]. Superfluidity in a Fermi gas in the entire BCS–BEC crossover was achieved and reported in 2004 [45–48]. A continuous thermodynamic superfluid transition was not observed until late 2004 [49]. A smoking gun of superfluidity came from the Ketterle group in 2005 which reported observation of vortex lattices, a macroscopic manifestation of quantum phenomena, from the BCS through BEC regimes [50]. Population (or spin) imbalance has been the second experimental parameter which has been explored in ultracold Fermi gases since 2006 [51, 52]. It is expected to lead to new phases such as phase separation and the exotic Fulde–Ferrell–Larkin–Ovchinnikov (FFLO) states [53–55]. Further parameters which have been gradually explored experimentally include geometric aspect ratio and dimensionality, mass imbalance, pairing symmetry such as p-wave, synthetic gauge fields and spin-orbit coupling, long range interactions as in dipolar molecules and magnetic atoms, as well as periodic potential, i.e., optical lattices.

There have been a few reviews on the subject of atomic Fermi gases. References [1] and [57] are the earliest reviews on this subject, emphasizing the similarity between Fermi gases and high T_c superconductivity as well as BCS–BEC crossover physics. Reference [58] reviewed the progress on the physics of degenerate Fermi gases from the theoretical perspective. Strong correlation effects in terms of many-body physics were only quickly mentioned as "other theoretical approaches". The review by Chin *et al.* [59] focuses more on Feshbach resonances, with a very brief touch on the experiments on BCS–BEC crossover. A few papers in the Varenna proceedings [60], as well as Ref. [2], also gave an review on the experimental and theoretical progress on atomic Fermi gases, without much emphasis on the pseudogap physics. It is the purpose of the current paper to give a more or less systematic review on the study of the pseudogap physics in cold atomic Fermi gases.

The rest of this paper is arranged as follows. In Section 2, we shall first introduce the concept of pseudogap in the context of high T_c superconductivity, and then provide examples of the pseudogap phenomena above and below T_c, and finally give an overview of the theoretical debate on the nature of the pseudogap. In Section 3,

we shall start by a summary of various theories of pairing fluctuations in the context of BCS–BEC crossover, and then present a particular pairing fluctuation theory for the pseudogap phenomena for a homogeneous system and later extend to Fermi gases in a trap. We shall end this section by presenting theoretical results on the thermodynamics and superfluid density. In Section 4, we shall show key results from the present pairing fluctuation theory on the pseudogap phenomena in both the 3D homogeneous case (Subsection 4.1) and in a trap (Subsection 4.3). In Subsection 4.2, we shall also give a summary of the applications of the present theory to high T_c superconductors with a d-wave pairing symmetry. In Section 5, we will present a series of experiments which show strong evidence or support of a pseudogap in unitary Fermi gases. While we focus mainly on population balanced two component Fermi gases, we shall show one case of population imbalanced Fermi gas experiment. In Section 6, we shall discuss the effect of particle-hole fluctuations and propose further experiments on pseudogap physics. Finally, we will conclude in Section 7.

2 What is a pseudogap? – Pseudogap phenomena in high T_c superconductors

2.1 What is a pseudogap?

We begin by introducing the concept of pseudogap, which has emerged since day one of high T_c superconductivity. In BCS theory, when the superconducting order parameter Δ becomes nonzero below the transition temperature T_c, a gap opens up at the Fermi level in the single particle excitation spectrum. The density of states (DOS) becomes zero within the gap. This gap originates purely from the order parameter and therefore vanishes at and above T_c. Soon after the high T_c superconductivity was discovered in cuprates, an excitation gap was observed already above T_c, below a higher temperature T^* (which is referred to as the pseudogap *crossover* temperature). Without phase coherence, such a gap does not lead to complete depletion of the DOS within the gap, but rather the DOS was only partially depleted. As T approaches T_c from above, the DOS drops quickly to zero at the Fermi level once phase coherence sets in as the system enters the superconducting state. In contrast to the true gap below T_c, *the gap observed experimentally above T_c has been referred to as a pseudogap*. Whether the pseudogap persists below T_c has been under debate.

The typical behavior of the DOS near the Fermi level for a pseudogapped superconductor is shown in Fig. 1 for various temperatures from T_c to slightly below T_c. The curves are calculated theoretically for an s-wave superconductor on a quasi-two dimensional (2D) lattice. From Fig. 1(a), one can see clearly a partial depletion of the DOS around the Fermi level ($\omega = 0$). As T lowers into the broken symmetry state, phase coherence sets in, and the DOS drops rapidly. At $T = 0.7T_c$, the depletion within the gap becomes almost complete so that the DOS looks like one in a strict BCS mean-field theory, with two sharp coherent peaks at the gap edges.

2.2 Pseudogap in the normal state above T_c

Above T_c, the pseudogap manifests itself in various physical quantities, including the $\mathrm{d}I/\mathrm{d}V$ characteristics in tunneling spectroscopy [62–65], specific heat [66, 67], dc resistivity [68–70], nuclear magnetic resonance (NMR) [71–76], infrared and ac conductivity [77–79], neutron scattering [80–82], Raman scattering [83–86], Nernst

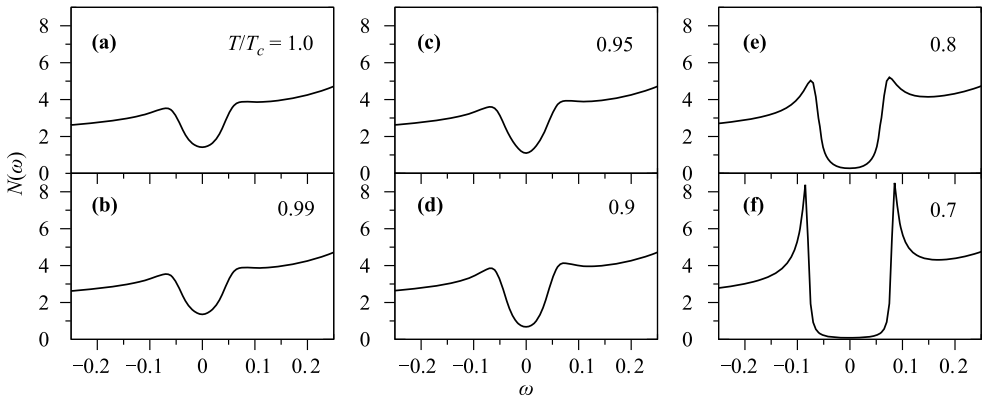

Fig. 1 Typical evolution of the density of states in the presence of a pseudogap for an s-wave superconductor as a function of temperature, calculated for an quasi-2D superconductor on a square lattice at quarter filling. Panels **(a)**–**(f)** correspond to various temperatures (as labeled) decreasing from $T = T_c$. The DOS drops rapidly as the system enters the superconducting state below T_c. At $T/T_c \sim 0.7$, as shown in (f), the DOS is close to a true gap as that of strict BCS theory. The frequency ω is in units of the 2D half band width. Reproduced from Ref. [56].

effect [87–90], spin susceptibility, etc., as a function of temperature. The most direct probe, of course, is the angle-resolved photoemission spectroscopy (ARPES) [61, 91, 92], which probes directly the spectral function $A(\boldsymbol{k}, \omega)$. Along the Fermi surface, the quasiparticle coherence peak position in the measured spectral function reveals directly the gap parameter. A review on various experiments on the pseudogap phenomena can be found in Ref. [7]. Here we only show a couple of examples to illustrate the pseudogap phenomena.

High T_c superconductors of the cuprates, such as $YBa_2Cu_3O_{7-\delta}$ (YBCO), $Bi_2Sr_2CaCu_2O_{8+\delta}$ (Bi2212) and $La_{2-x}Sr_xCuO_4$ (LSCO), have a layered structure, with charge carriers moving in the copper-oxide planes. The electron transport along the c-axis (i.e., the direction perpendicular to the planes) is largely incoherent. This makes the cuprates quasi-2D materials. While the parent compounds are insulating antiferromagnets, superconductivity occurs at low T upon hole doping [93]. Within the superconducting (ab-) planes, it is now known that the order parameter Δ of the cuprate superconductors has a $d_{x^2-y^2}$ symmetry, such that $\Delta = \Delta_0(\cos k_x - \cos k_y)/2$, where we have set the in-plane lattice constant a to unity. Thus the gap has a maximum in the anti-nodal directions near $(\pi, 0)$, whereas it closes in the nodal directions from Γ to (π, π) in the Brillouin zone (BZ). The order parameter changes sign across the nodal points along the Fermi surface.

Shown in Fig. 2(a) is a schematic phase diagram for the cuprate superconductors. The transition temperature T_c reaches a maximum around doping concentration $x = 0.155$. There is a temperature range between T_c and T^* in the underdoped regime where a finite pseudogap exists. Shown in Fig. 2(b) are the ARPES measurements of the excitation gap near $(\pi, 0)$ for Bi2212 at different doping concentrations. At optimal doping ($T_c = 87$ K sample), the gap closes roughly at T_c, similar to that predicted in BCS theory. However, for the underdoped samples, it is clear that the gap persists at very high T. This is the most direct measurement, and hence evidence of the existence, of a pseudogap above T_c.

In Fig. 3, we present, as an example, typical normal-insulator-superconductor (SIN) tunneling spectra measured for an underdoped cuprate superconductor as a function of temperature, using scanning tunneling microscopy (STM). Here the $\mathrm{d}I/\mathrm{d}V$ characteristics can be regarded as the DOS, but broadened by thermal effects. In sharp contrast with a BCS mean-field true gap, the pseudogap does not close even at T^*. But rather, the coherence peaks broaden and the DOS fills in with increasing T. At T^*, the sign of DOS depletion disappears and so does the pseudogap. The way the pseudogap

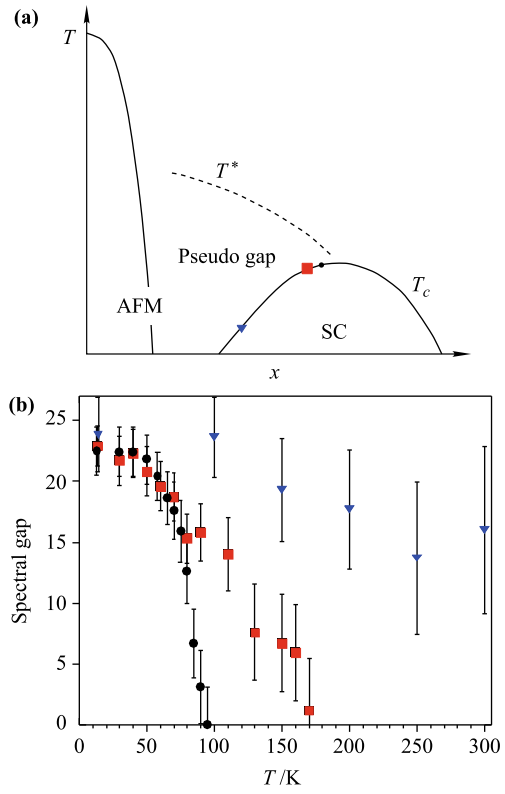

Fig. 2 **(a)** Schematic phase diagram for the cuprate superconductors (The horizontal axis is the hole doping concentration), and **(b)** ARPES measurement of the temperature dependence of the excitation gap at $(\pi, 0)$ in a near-optimal $T_c = 87$ K sample (●), and underdoped 83 K (■) and 10 K (▼) samples. The gap values were determined via leading edge shift from the Fermi level. The units for the gap are meV. Panel (b) is reproduced from Ref. [61].

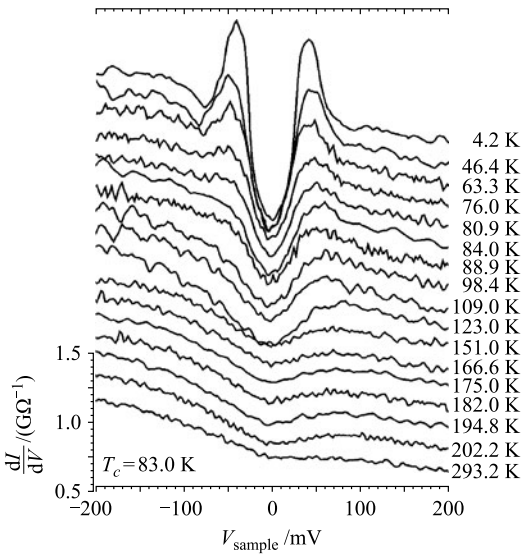

Fig. 3 Typical tunneling spectra for an underdoped cuprate superconductor as a function of temperature. Shown data were measured on an underdoped Bi2212 sample of $T_c = 83$ K. The horizontal axis is the bias. The conductance scale corresponds to the 293 K spectrum, the other spectra are offset vertically for clarity. Reproduced from Ref. [63].

disappears at high T is a clear distinction from that of a true gap in a weak coupling BCS superconductor, which shrinks in magnitude to zero at T_c.

Similar behavior can be found in the ARPES energy distribution curves (EDC) for underdoped samples as well [61, 91]. Usually, an ARPES EDC curve consists of a quasiparticle coherence peak on top of an incoherent background. At $T \ll T_c$, the coherence peak is sharp and pronounced. Once the temperature rises above T_c, for an underdoped sample, it becomes broadened quickly, and the spectral weight under the peak decreases with T rapidly, until it merges with the large incoherent background. At the same time, the peak location almost does not move with T. This can be seen in Fig. 4. The EDC curves in Figs. 4(a) and (b) were taken along the cut in the Brillouin zone shown in Fig. 4(c), which goes across the Fermi level. Panels (a) and (b) correspond to low $T \ll T_c$ and above T_c cases, respectively, with curves of the same $\boldsymbol{k}$ lined up together. As the cut goes through the Fermi surface, the coherence peak reaches the minimum quasiparticle excitation energy, as determined by the excitation gap $\Delta_{\boldsymbol{k}}$. It is obvious that the coherence peak in the pseudogap case is much broader and less pronounced than its superconducting counterpart.

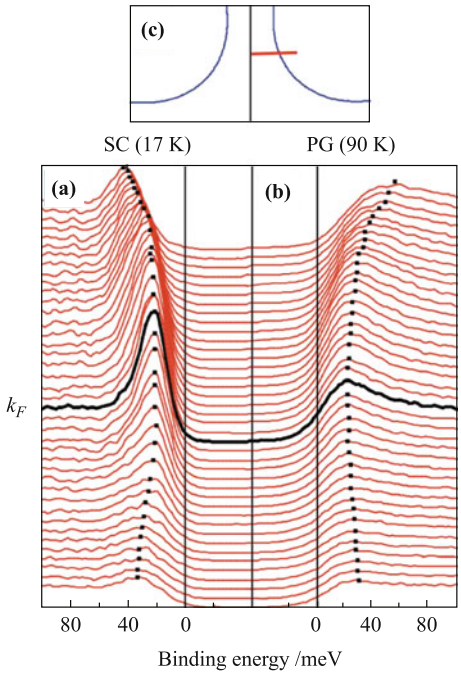

Fig. 4 Comparison of EDCs between **(a)** the superconducting state (T = 17 K) and **(b)** the pseudogap phase (T = 90 K) for a Bi2212 film with T_c = 80 K for the cut in the zone shown in **(c)**. The thick curves in (a) and (b) correspond to where the cut goes through the Fermi surface. Here SC and PG denote superconducting and pseudogap state, respectively. Reproduced from Ref. [92].

2.3 Pseudogap in the superfluid state below T_c

Figures 2–4 and most experimental measurements show clear evidence of the existence of a pseudogap at and above T_c. It is a natural question to ask how the pseudogap above T_c and the superconducting gap below T_c connect to each other at T_c. There have been intensive debates on this issue over the years. The answer to this important question depends on the interpretation of the pseudogap in different theories. Despite the differences from one theory to another, one can think of two possibilities in general. One possibility is that the pseudogap becomes the superconducting gap instantly once the system enters the superconducting state across T_c. The other is that the order parameter or the superconducting gap increases gradually from zero at T_c. For the former, one would see a first order phase transition and a jump in the order parameter and superfluid density across T_c. For the latter possibility, the pseudogap necessarily persists into the superfluid state, in order to keep the total excitation gap smooth across T_c as observed in ARPES data and other experiments. Given these rather obvious differences between these two possibilities, superfluid density (n_s/m) or in-plane London penetration depth (λ) measurements seem to have unambiguously ruled out the former possibility. Indeed, superfluid density $n_s/m \propto \lambda^{-2}$ vanishes continuously as T approaches T_c from below in bulk cuprate superconductors.

At a more concrete level, compatible with the first possibility may be a school of microscopic theories which consider the pseudogap above T_c as a signature of a competing hidden order, such as the d-density wave (DDW) order [94], the staggered orbital current [95–97], loop current order [98, 99], etc. Given the hidden order assumption, a natural prediction would be that the hidden ordered phase gives way completely to the superconducting order across T_c, as in most other phase transitions. However, if this is true, not only a first order transition is necessary, but also it would take a miracle for the total excitation gap to remain so smooth across T_c as observed experimentally. Then to pass the experimental test, these hidden order theories may also need to associate themselves with the second possibility, namely the hidden order parameter (and thus the pseudogap) survives the superconducting phase transition and coexists with the superconducting order below T_c. Together they contribute to the total excitation gap.

Among the second possibility, there are different scenarios which give rise to different interpretations and different temperature dependencies of the pseudogap. These differences are associated with the origins of the pseudogap in these theories or conjectures. In order to

fit the specific heat data for underdoped superconductors, Loram and coworkers [66, 100, 101] contemplated that the pseudogap below T_c may take its value at (and above) T_c such that it is relatively temperature independent. As a consequence, (the magnitude of) the order parameter (Δ_{sc}) is much smaller than the total excitation gap (Δ) at all $T < T_c$ for an underdoped cuprate superconductor. We note that this was a rather simple recipe *without any theoretical justification*. Among microscopic theories, while the competing hidden order theories may be associated with the second possibility, a most natural school of theories in this category would be the *precursor superconductivity*, in which the pseudogap is a precursor to the superconductivity and originates from the same pairing as that causes the superconducting order at low T. We will elaborate further on this in the next subsection.

To probe the pseudogap below T_c, if it does exist, the best way is arguably to suppress the order parameter. Luckily, this can be achieved inside a vortex core. Figure 5 shows STM measurements of the $\mathrm{d}I/\mathrm{d}V$ characteristics of an underdoped Bi2212 sample inside and outside a vortex core at very low T. Outside the vortex core, the order parameter is large at low T, and there are sharp peaks at the gap edges (dashed curve). At the center of the vortex core, the superconducting order parameter is suppressed to zero (solid curve). Nevertheless, it is clear that the $\mathrm{d}I/\mathrm{d}V$ curve shows a strong depletion of the DOS within the peaks. The peak locations are roughly the same as those outside the core. Of course, such a depletion is absent above the pseudogap crossover temperature T^*. Therefore, this plot serves as evidence of pseudogap below T_c in an underdoped cuprate. Indeed, this can be naturally explained within a pairing fluctuation theory [23]; In addition to noncondensed pairs, the magnetic field inside the vortex core causes the originally condensed pairs lose phase coherence and thus contribute to the pseudogap rather than the order parameter [102]. On the other hand, as one may notice, in order for the

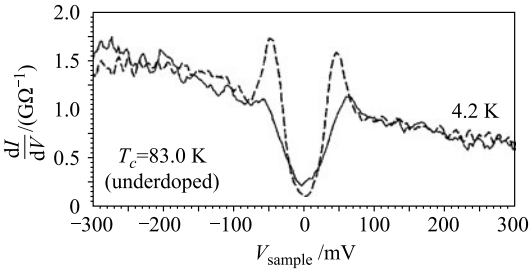

Fig. 5 STM measurements of the $\mathrm{d}I/\mathrm{d}V$ characteristics of an underdoped Bi2212 sample inside (*solid*) and outside (*dashed*) a vortex core at low $T = 4.2$ K. Here $T_c = 83$ K. $\mathrm{d}I/\mathrm{d}V$ is proportional to the density of states. Reproduced from Ref. [62].

competing hidden order theories to explain the survival of the total gap at the center of the vortex core at very low T, one would have to assume that the superconducting order is converted into hidden order parameter by the magnetic field. This, however, is very unnatural.

2.4 Theoretical debate about the nature of the pseudogap

The pseudogap phenomena is widespread in high T_c superconductivity experiments. However, a consensus of its origin is yet to be reached. There have been many different theories attempting to explain the nature of the pseudogap. Most of these theories only provide qualitative pictures, incapable of quantitative calculations.

Early models include the resonating valence bond (RVB) theory of Anderson [103, 104] and the closely related spin-charge separation idea [105, 106]. In these theories, the pseudogap originates from the spin gap of the antiferromagnetic spin pairing (i.e., the spinon pairing). Despite the well established phenomena of spin-charge separation in 1D, so far there has been no experimental support for spin-charge separation in 2D, not to mention 3D.

About the same time, Uemura and coworkers [107, 108] noticed possible connections between the cuprate superconductivity and BEC via the well-known Uemura plot of T_c versus superfluid density n_s/m^*. This has been used to suggest that the cuprates have to do with BCS–BEC crossover. In an attempt to explain the pseudogap phenomena, Lee and coauthors [16, 17] proposed a boson-fermion model. The pseudogap phenomena was then explored using the BCS–BEC crossover idea in 3D continuum [18–22] or the negative-U Hubbard model on a lattice [26–29], assuming an s-wave pairing symmetry. These theories belong to the school of precursor superconductivity, in which the pseudogap above T_c and the superconducting gap below T_c originate from the same pairing interaction, and thus the pseudogap in the normal state is a precursor to superconductivity below T_c. A theory of the broken symmetry state and the presence of the pseudogap below T_c, especially for d-wave pairing, was not available until the work of Refs. [23–25].

It is worth mentioning that in a very recent work [109], Mishra and coworkers showed that a pseudogap which is not associated with pairing would suppress T_c to zero. Therefore, they concluded that the pseudogap observed in the cuprates must be due to pairing.

Compatible with but distinct from the precursor superconductivity school are theories based on phase fluctuations such as that of Emery and Kivelson [110] and the QED3 theory of Tesanovic and coworkers [111]. The

former addresses mainly spin-wave type of phase fluctuations whereas the latter has an emphasis on vortex fluctuations. In both theories, the pseudogap originates from a pairing field without phase coherence; the pairing field emerges at T^* but the phase coherence does not lock in until a lower temperature T_c. The strong Nernst signals observed above T_c in underdoped cuprates [87–89] may be regarded as a support for the latter theory. On the other hand, it should be noted that the Nernst effect data can be explained within a pairing fluctuation theory as well [90, 112].

Both the spin gap scenarios as in RVB and spin-charge separation and charge gap scenarios as in precursor superconductivity and phase fluctuation pictures have to do with pairing in the particle-particle channel. A big departure from this common feature are the competing hidden order ideas, mentioned in Subsection 2.3, which take the pseudogap as a hidden order parameter. For example, the DDW order is associated with the particle-hole channel. The staggered current and loop current order are not related to pairing, either. They rely on the underlying quasi-2D lattice structure of the cuprates.

The RVB and spin-charge separation ideas can be traced back to the fact that the parent compounds of the cuprate superconductors are insulating antiferromagnets in the Mott state, with an underlying quasi-2D, layered lattice structure. The DDW, staggered current and loop current ideas have also to do with the underlying lattice structures, which are apparently not pertinent to the atomic Fermi gases in a big single trap. Deeper than but closely related to the pseudogap phenomena is the mechanism of superconductivity in the cuprates, namely, what provides the glue for the electrons to pair up.

Luckily, for atomic Fermi gases, the underlying pairing interaction is known and can be precisely manipulated experimentally. While one may continue to debate on the origin of the pseudogap phenomena in the cuprates, as far as the atomic Fermi gases are concerned, this fact does make the pairing fluctuation theory the most natural candidate for the theory of the superfluidity and pairing.

3 Pairing fluctuation theory for the pseudogap

3.1 Various pairing fluctuation theories for BCS–BEC crossover

Pairing fluctuation theories belong to the school of precursor superfluidity. There are different pairing fluctuation theories. Nevertheless, common to these theories are strong pairing fluctuations or pairing correlations already above T_c, which necessarily cause deviation of the system behavior from those described by the BCS mean-field theory. The first thing that has been looked into is the superfluid transition temperature T_c. Not all of these theories contain a pseudogap in their single particle excitation spectrum, nor are they all self-consistent. As the pairing strength varies, a pairing fluctuation theory is often used to address the BCS–BEC crossover problem, and thus is often referred to as a BCS–BEC crossover theory as well. Note that from this section on, we will use the term "superfluidity" in place of "superconductivity", in order to be appropriate for both superconductors and charge neutral superfluids.

The very first work on finite temperature BCS–BEC crossover, by Noziéres and Schmitt–Rink (NSR) [15] in 1985, can be regarded as the earliest pairing fluctuation theory. However, in the NSR theory, only bare Green's functions are involved so that the pairing fluctuations induced self energy does not feed back into the T_c equation. As a consequence, pseudogap does not appear in the NSR theory. Although one may find features of pseudogap via further calculation of the spectral function with the self-energy included, this procedure certainly breaks self-consistency. Indeed, not including the self energy in the T_c equation itself introduces inconsistency. For example, the T_c equation is inconsistent with the condition

$$\frac{\partial \Omega_S}{\partial \Delta} = 0 \tag{1}$$

as T_c is approached from below, where Ω_S is the thermodynamic potential in the superfluid state. Sá de Melo *et al.* [18] obtained identical equations as NSR, using a Saddle point approximation plus Gaussian fluctuations. There have been many studies in the literature using a similar approximation [19]. Milstein *et al.* [113] used a similar treatment but within a two-channel model. Indeed, it has turned out that the saddle point approximation with Gaussian fluctuations and the NSR approximation are equivalent. With a narrow Feshbach resonance in a two-channel model, Ohashi and Griffin [114] caculated T_c using the NSR approximation. Strinati and coworkers [115, 116] also followed the NSR calculation found the same T_c and number equations as NSR. There are other pairing fluctuation theories on BCS–BEC crossover based on the NSR approximation. Noticeably, rather than fixing the inconsistency in the T_c equation, Hu and Drummond [117] proposed to add an extra term in the number equation. This necessarily leads to two unphysical results: (i) This extra term does not exist above T_c, so that it will give rise to a different T_c and chemical potential μ, depending on whether T_c is approached from

above or below. (ii) In a trap, a uniform global chemical potential requires that the density jumps across the edge of the superfluid core. In fact, should the T_c equation is fixed so that Eq. (1) is satisfied, this extra term would vanish automatically. More systematic and detailed comparison between the NSR-based theories and the pairing fluctuation theory which we will present soon below can be found in Ref. [118].

Using a GG scheme for the T-matrix approximation, which is sometimes referred to as a conserving approximation, Haussmann [32] and Tchernyshyov [33] *et al.* developed a different kind of pairing fluctuation theory, which leads to a substantially lower T_c than others, especially in the BCS through unitary regimes. This is primarily because the GG scheme double counts certain self energy diagrams. This theory is rather similar to the FLEX approximation of Scalapino and coworkers [119, 120] for the cuprates. Recently, Haussmann *et al.* [121] improved upon the NSR theory but found unphysical non-monotonic first-order-like behavior in the temperature dependence of entropy, $S(T)$.

It should be emphasized that none of these above mentioned theories contained pseudogap self energy in the T_c equation. All NSR based theories essentially inherit the inconsistency of NSR treatment as well.

A pairing fluctuation theory which does contain a pseudogap was developed by the Levin group. Levin and coworkers [20–22] did intensive numerical study and found that a pseudogap opens up as T approaches T_c from above once the pairing correlation self energy is fed back into the T_c equation. Chen, Kosztin and coworkers [23, 25] extended this work into a systematic theory for the superfluid state, and applied it to d-wave cuprate superconductors. With proper inclusion of low dimensionality and lattice effects [24], Chen *et al.* [23] found an excellent (semi-quantitative) agreement of their computed cuprate phase diagram with that observed experimentally. This theory also gives a very natural explanation of the anomalous quasi-universal behavior of the superfluid density as a function of T for different hole doping concentrations. In contrast to other theories mentioned above, pseudogap is a natural unavoidable consequence of strong pairing correlations in this theory.

Now with experimental evidence of a pseudogap in atomic Fermi gases, more people are finding in their theories evidence of a pseudogap [122–124]. Various quantum Monte Carlo simulations are also finding a pseudogap at unitarity above T_c.

3.2 Pairing fluctuation theory for the pseudogap

In this subsection, we will present a particular pairing fluctuation theory, in which the pairing correlation self energy is fed back into the T_c and gap equation in a self-consistent fashion.

As in all pairing fluctuation theories, the key difference between this theory and the BCS mean field theory is that it includes finite center-of-mass momentum pairing. It is the finite momentum pairing that will give rise to a self energy beyond the strict BCS mean-field treatment.

What makes this theory unique is that finite momentum pairs and single particles are treated on an equal footing. As a consequence, these finite momentum pairs will cause a single particle excitation gap without phase coherence. In fact, the physical picture here is very intuitive. When strong pairing correlations are present, to excite a single fermion above T_c, one necessarily has to pay extra energy in order to break the pairing. This extra energy is associated with the pseudogap. In the BCS limit, this extra energy is negligible. However, in the BEC limit, stable two-body bound pairs will form at high T so that one has to pay at least the binding energy to break the pairs. In the unitary or crossover regime, the pairs are meta-stable with a zero two-body binding energy so that the pseudogap is most pronounced. Needless to say, very much like the superfluid order parameter, the pseudogap is a many-body effect. While the pseudogap persists deep into the BEC regime, where a Fermi surface no longer exists, the big two-body binding energy may obscure the pseudogap effects. While the low energy excitations are Bogoliubov quasiparticles and finite momentum pairs for the BCS and BEC limits, respectively, a mix of both types necessarily takes place in the crossover regime. This is a requirement of the *smoothness* of the crossover.

The derivation of this theory [56] follows the early work of Kadanoff and Martin [125]. Through the equation of motion approach with a truncation of the infinite series of equations at the three-particle level, and decomposing the three particle Green's function G_3 into a sum of products of single particle Green's function G and two-particle Green's function G_2, we rigorously derived our self-consistent set of equations, with reasonable simplifications. While our equations may be conveniently cast diagrammatically into a T-matrix approximation, we emphasize that this theory is *not* a diagrammatic approach. For example, the pair susceptibility χ consists of a mix of bare Green's function G_0 and full Green's function G. This mix is *not an ad hoc diagrammatic choice*, but rather a natural consequence of the equation of motion approach. A main and nice feature of this theory is that it naturally recovers the BCS-Leggett result at zero T and in the BCS limit. In addition, throughout the superfluid

phase, our Green's function and the equations take the BCS form, except for the extra pseudogap contribution in the quasiparticle dispersion. Finally, the pseudogap (squared) is directly proportional to the density of finite momentum pairs, so that it provides a good measure of the contributions of finite momentum pairing fluctuations.

Instead of giving a full derivation of the theory, which can be found elsewhere [56], here we only give a summary and present the key equations so that we can focus on the physical picture. In addition, here we only consider the one-channel model, which is appropriate for high T_c superconductors as well as atomic Fermi gases with a wide Feshbach resonance. A two-channel version of this theory can be found in Refs. [1, 126].

It is known that superfluidity concerns primarily the particle-particle channel. The main processes are summarized in the Feynman diagrams shown in Fig. 6. Here the finite momentum T-matrix t_{pg} may be regarded as (the central part of) a two-particle propagator, and the dashed line represents non-propagating, zero-momentum pairs in the condensate. The self-energy Σ of the single fermions comes from scattering with condensed and non-condensed pairs. Alternatively, a fermion may decay into a pair and a hole, which then recombine at a later point in spacetime, as shown in the second line in the figure. From the first line, it is not hard to conclude that the T-matrix can be regarded as a renormalized pairing interaction. Indeed, summing up the ladder diagrams, one obtain

$$t_{pg}(Q) = \frac{U}{1 + U\chi(Q)} \tag{2}$$

with the same dimensionality as the interaction, where we have assumed a separable pairing interaction $V_{\boldsymbol{k},\boldsymbol{k}'} = U\varphi_{\boldsymbol{k}}\varphi_{\boldsymbol{k}'}$, with $\varphi_{\boldsymbol{k}} = 1$ for a short range contact potential in atomic Fermi gases and $\varphi_{\boldsymbol{k}} = \cos k_x - \cos k_y$ for d-wave cuprate superconductors [127]. Here the pair susceptibility

$$\chi(Q) = \sum_K G_0(Q-K)G(K)\varphi^2_{\boldsymbol{k}-\boldsymbol{q}/2} \tag{3}$$

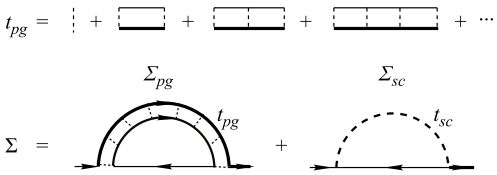

Fig. 6 Feynman diagrams of the particle-particle scattering T-matrix t_{pg} and the single particle self energy Σ. The self energy Σ contains two contributions, from the condensate and finite momentum pairs, respectiveily.

For clarity, a four-vector notation has been used, i.e., $K = (\mathrm{i}\omega_l, \boldsymbol{k})$, $Q = (\mathrm{i}\Omega_n, \boldsymbol{q})$, $\sum_K \equiv T\sum_l \sum_{\boldsymbol{k}}$, etc., where $\Omega_n = 2n\pi T$ and $\omega_l = (2l+1)\pi T$ are even and odd Matsubara frequencies, respectively. Here and throughout we shall use the natural units $\hbar = k_{\mathrm{B}} = 1$ and set the volume to unity.

From Fig. 6, it is straightforward to write down the self-energy Σ and its superconducting component Σ_{sc} and pseudogap component Σ_{pg}, as follows:

$$\Sigma(K) = \Sigma_{sc}(K) + \Sigma_{pg}(K) \tag{4a}$$

$$\Sigma_{sc}(K) = -\Delta^2_{sc}G_0(-K)\varphi^2_{\boldsymbol{k}} = \frac{\Delta^2_{sc}\varphi^2_{\boldsymbol{k}}}{\mathrm{i}\omega_l + \xi_{\boldsymbol{k}}} \tag{4b}$$

$$\Sigma_{pg}(K) = \sum_Q t_{pg}(Q)G_0(Q-K)\varphi^2_{\boldsymbol{k}-\boldsymbol{q}/2} \tag{4c}$$

where $\xi_{\boldsymbol{k}} = \epsilon_{\boldsymbol{k}} - \mu$ is the free fermion dispersion measured with respect to the Fermi level.

At this point, an approximation is needed in order to simplify the final result. Notice that pairing instability condition, i.e., the Thouless criterion, $t^{-1}_{pg}(0) = 0$, implies that the main contribution in Eq. (4c) comes from the vicinity of $Q = 0$. This leads to a good mathematical simplification over the complicated convolution,

$$\begin{aligned}\Sigma_{pg}(K) &\approx \left[\sum_Q t_{pg}(Q)\right] G_0(-K)\varphi^2_{\boldsymbol{k}} \\ &= -\Delta^2_{pg}G_0(-K)\varphi^2_{\boldsymbol{k}}\end{aligned} \tag{5}$$

where we have defined the pseudogap Δ_{pg} via

$$\Delta^2_{pg} = -\sum_Q t_{pg}(Q) \tag{6}$$

Now it is clear that, under approximation Eq. (5), we have the total self energy in the BCS form,

$$\Sigma(K) = -\Delta^2 G_0(-K)\varphi^2_{\boldsymbol{k}} \tag{7}$$

where we have defined a total excitation gap Δ via

$$\Delta^2 = \Delta^2_{sc} + \Delta^2_{pg} \tag{8}$$

Therefore, one immediately concludes that the full Green's function $G(K)$ also takes the BCS form,

$$G(K) = \frac{u^2_k}{\mathrm{i}\omega_l - E_k} + \frac{v^2_k}{\mathrm{i}\omega_l + E_k} \tag{9}$$

where $E_k = \sqrt{\xi^2_{\boldsymbol{k}} + \Delta^2\varphi^2_{\boldsymbol{k}}}$ is the dispersion of the Bogoliubov quasiparticles, and $u^2_{\boldsymbol{k}}, v^2_{\boldsymbol{k}} = \frac{1}{2}(1 \pm \xi_{\boldsymbol{k}}/E_{\boldsymbol{k}})$ are formally the usual BCS coherence factors.

Upon substituting the expressions for G_0 and G into the Thouless criteria, $U^{-1} + \chi(0) = 0$, one obtains immediately the gap (or T_c) equation after carrying out the

Matsubara summation,

$$1+U\sum_{\boldsymbol{k}}\frac{1-2f(E_{\boldsymbol{k}})}{2E_{\boldsymbol{k}}}\varphi_{\boldsymbol{k}}^2=0 \tag{10}$$

where $f(x)$ is the Fermi distribution function. For a short range contact potential with $\varphi_{\boldsymbol{k}}=1$, as in atomic Fermi gases, one may conveniently regularize the ultraviolet divergence via the relation [128]

$$\frac{m}{4\pi a}=\frac{1}{U}+\sum_{\boldsymbol{k}}\frac{\varphi_{\boldsymbol{k}}^2}{2\epsilon_{\boldsymbol{k}}} \tag{11}$$

based on the Lippmann–Schwinger equation, so that the interaction strength U is replaced with (the inverse of) the low energy s-wave scattering length a, which is a widely used experimental parameter in the AMO community. In this way, the gap equation becomes

$$\frac{m}{4\pi a}+\sum_{\boldsymbol{k}}\left[\frac{1-2f(E_{\boldsymbol{k}})}{2E_{\boldsymbol{k}}}-\frac{1}{2\epsilon_{\boldsymbol{k}}}\right]\varphi_{\boldsymbol{k}}^2=0 \tag{12}$$

Note that Eq. (11) defines a critical coupling U_c, which is more familiar to the condensed matter community; U_c corresponds to the threshold for two fermions to form a bound state in vacuum, where the scattering length a diverges,

$$U_c=-1\Big/\sum_{\boldsymbol{k}}\frac{\varphi_{\boldsymbol{k}}^2}{2\epsilon_{\boldsymbol{k}}} \tag{13}$$

Obviously, U_c depends on the ultraviolet cutoff momentum in $\varphi_{\boldsymbol{k}}^2$. It is worth mentioning that in 2D and the contact limit in 3D, U_c goes to zero for an s-wave pairing interaction [129].

Now it should be emphasized that it is the mixed form of the pair susceptibility χ in Eq. (3) that gives rise to the BCS form in the gap equation (10). This is very satisfying since it is known that BCS theory works well in the weak coupling regime. Such a feature was already recognized in the early paper by Kadanoff and Martin [125]. Throughout the entire BCS–BEC crossover, this BCS form of gap equation reproduces the BCS–Leggett ground state [14]. This is an important merit of the present pairing fluctuation theory, since, while one may argue that the BCS–Leggett ground state is not perfect in the BEC regime, it has nonetheless been a basis for various theoretical works. It is apparent that the gap equation in other competing T-matrix approximations with a G_0G_0 or GG in the pair susceptibility will deviate substantially from the BCS form.

Given the full Green's function Eq. (9), it is straightforward to write the fermion number constraint,

$$n=2\sum_{\boldsymbol{k}}\left[v_k^2+\frac{\xi_{\boldsymbol{k}}}{E_{\boldsymbol{k}}}f(E_{\boldsymbol{k}})\right] \tag{14}$$

which is the number equation.

Equations (10), (9) and (6) now forms a closed set of self-consistent equations, which can be used to solve for T_c and μ, and Δ_{pg} at T_c, or for Δ, μ, and Δ_{pg} for $T<T_c$. To simplify and facilitate the computation of Eq. (6), we Taylor-expand the inverse T matrix after analytic continuation, $\mathrm{i}\Omega_n\to\Omega+\mathrm{i}0^+$, as

$$t_{pg}^{-1}(\Omega,\boldsymbol{q})=Z\left(\Omega-\frac{q^2}{2M^*}+\mu_{\rm pair}\right) \tag{15}$$

at the lowest order in Ω and $\boldsymbol{q}$. A more elaborate treatment which includes higher order terms such as Ω^2 as well as the imaginary part can be found in Ref. [56]. Use of such higher order expansion is made in cases where it makes a substantial (quantitative) difference [130, 131]. Here the inverse residue Z, the effective pair mass M^*, and the effective pair chemical potential $\mu_{\rm pair}$ can be obtained in the process of the expansion. One can immediately extract the pair dispersion $\Omega_{\boldsymbol{q}}=q^2/(2M^*)-\mu_{\rm pair}$. It now follows that

$$Z\Delta_{pg}^2\approx\sum_{\boldsymbol{q}}b(\Omega_{\boldsymbol{q}}) \tag{16}$$

where $b(x)$ is the usual Bose distribution function. Evidently, Eq. (16) suggests that Δ_{pg}^2 represents the density of finite momentum pairs (up to a nearly constant coefficient).

Typical behaviors of the T-matrix $t_{pg}(\Omega,\boldsymbol{q})$ and its inverse are shown in Fig. 7. The curves are calculated for a 3D unitary Fermi gas at T_c, with a Lorentzian type of pairing potential, $\varphi_{\boldsymbol{k}}^2=[1+(k/k_0)^2]^{-1}$ at $k_0/k_F=4$ and $q/k_F=0.3$. From the lower panel, one can see that the Taylor expansion of the inverse T-matrix, $t_{pg}^{-1}(\Omega,\boldsymbol{q})$, up to the order of Ω^2, agrees with the real part of the full curve very well near the dispersion relation $\Omega\approx\Omega_{\boldsymbol{q}}$, where the imaginary part, $\mathrm{Im}\,t_{pg}^{-1}(\Omega,\boldsymbol{q})$, becomes very small. This leads to a sharp resonance peak in $\mathrm{Im}\,t_{pg}(\Omega,\boldsymbol{q})$ at $\Omega\approx\Omega_{\boldsymbol{q}}$. This peak becomes sharper for smaller q and at lower T, as expected. When the order parameter develops below T_c, for $q=0$, there is an extended range of Ω at which $\mathrm{Im}\,t_{pg}^{-1}(\Omega,0)$ vanishes. This is an effect of a finite excitation gap.

From the expansion Eq. (15), it is easy to see that the Thouless criterion requires

$$\mu_{\rm pair}=0,\quad \text{for}\quad T\leqslant T_c \tag{17}$$

which is precisely the BEC condition of the (bosonic) fermion pairs. Therefore, it is transparent that *the present pairing fluctuation theory unifies BCS theory and Bose–Einstein condensation* using the BCS–BEC crossover picture; They are two sides of the same coin. Such a unification has not been made so obvious in other

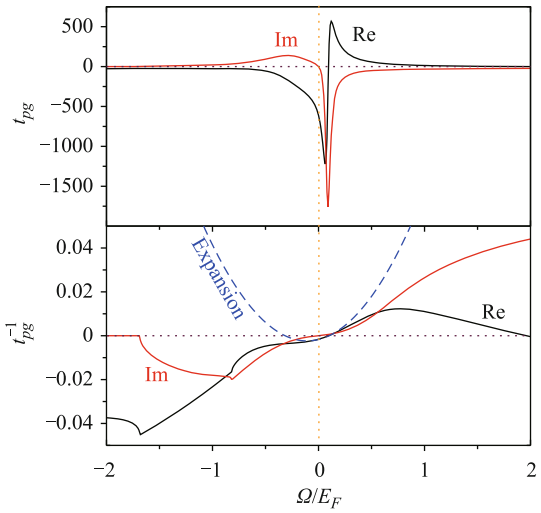

Fig. 7 Typical behavior of the T-matrix and its inverse. Shown are calculated at unitarity $U = U_c$ at T_c, for a 3D continuum case with a finite range of interaction of the Lorentzian type $\varphi_{\boldsymbol{k}}^2 = [1 + (k/k_0)^2]^{-1}$, with $k_0/k_F = 4$ and pair momentum $q/k_F = 0.3$. Here Re and Im denote real and imaginary parts, respectively. The blue dashed curve is from the expansion of the inversion T-matrix, which coincides with the full Re t_{pg}^{-1} curve in the neighborhood of $\Omega = \Omega_{\boldsymbol{q}}$.

competing pairing fluctuation theories. Technically, it is the Taylor expansion Eq. (15) that has made this unification transparent; a similar expansion has not been seen in competing theories.

Indeed, as shown in Fig. 8, for different $T \leqslant T_c$ (solid curves), the real part Re $t_{pg}^{-1}(\Omega, \boldsymbol{q} = \boldsymbol{0})$ always goes through the origin. However, for $T > T_c$ (dashed curves), this is no longer true. The nonzero intercept $t_{pg}^{-1}(0,0) = Z\mu_{\rm pair}$ determines the effective pair chemical potential above T_c.

In fact, there are various situations where we need to know the approximate value of the pseudogap above T_c.

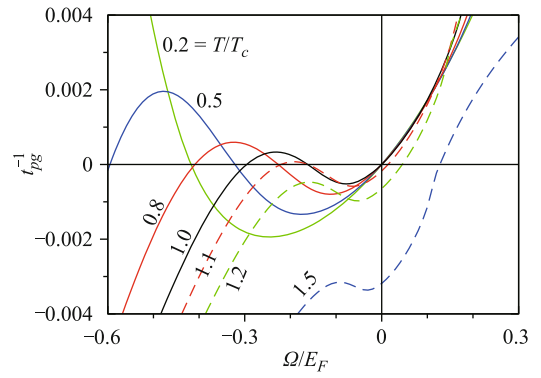

Fig. 8 Typical behavior of the real part of the inverse T-matrix $t_{pg}^{-1}(\Omega, 0)$ near $\Omega = 0$ for different T, as labeled, below (*solid*) and above T_c (*dashed curves*). Shown are results calculated at unitarity $U = U_c$, for a 3D continuum case with a finite range of interaction of the Lorentzian type $\varphi_{\boldsymbol{k}}^2 = [1 + (k/k_0)^2]^{-1}$, with $k_0/k_F = 4$.

In such a case, we need to extend the gap equation (10) or (12) to situations above T_c, as

$$\frac{m}{4\pi a} + \sum_{\boldsymbol{k}} \left[\frac{1 - 2f(E_{\boldsymbol{k}})}{2E_{\boldsymbol{k}}} - \frac{1}{2\epsilon_{\boldsymbol{k}}} \right] \varphi_{\boldsymbol{k}}^2 = Z\mu_{\rm pair} \tag{18}$$

The pseudogap equation is still given by Eq. (16) but with a nonzero $\mu_{\rm pair}$, along with the number equation (14). Since $\Delta_{sc} = 0$ above T_c, it is clear that the three unknowns are now ($\Delta_{pg} = \Delta$, μ, $\mu_{\rm pair}$), as compared to (Δ_{pg}, μ, Δ_{sc}) below T_c.

It should be pointed out that as T increases above T_c, the T matrix $t_{pg}(Q)$ no longer diverges at $Q = 0$. Therefore, Eq. (5) is no longer a good approximation for the pseudogap self energy $\Sigma_{pg}(K)$. In this sense, the use of the extended gap equation (18) should be restricted to a temperature regime not far above T_c, where $-\mu_{\rm pair}$ is still very small.

Generalization of the above equations to population imbalanced as well as mass imbalanced situations is straightforward, which can be found in Refs. [130–135].

Finally, a few remarks are in order. The pseudogap self energy given in Eq. (4c) formally contains all contributions at the T-matrix level. However, by Eq. (5), the pseudogap self energy is approximated by a BCS-like, off-diagonal, coherent form. When the pseudogap Δ_{pg} vanishes, the pseudogap self energy is gone. Therefore, the diagonal incoherent contributions are dropped out. The incoherent contributions, $\delta\Sigma(K)$, is dominant in the weak coupling BCS limit, and becomes less important in the intermediate through strong coupling BEC regimes. It mainly causes a chemical potential shift, as well as a slight fermion mass renormalization. Such contributions are usually neglected in the study of superconductivity. Nevertheless, for atomic Fermi gases, as the strong couplings regime becomes accessible, it is known that these contributions have a substantial *quantitative* impact on the so-called beta factor at unitarity [136], which is defined as $1 + \beta = \mu(0)/E_F$, where $\mu(0)$ and E_F are the zero T chemical potential at unitarity and the noninteracting Fermi energy, respectively. Without the incoherent contributions, the present theory produces the same prediction as the BCS mean-field result, $\beta \approx -0.41$, whereas the experimental values and quantum Monte Carlo (QMC) simulation results are found between -0.5 and -0.7 [49, 137, 138]. When the incoherent contributions are included, theoretical calculations of Perali *et al.* found $\beta \approx -0.545$, in better agreement with experiment, as expected. Here our attention is focused mainly on the moderate and strong coupling regimes, where the pseudogap effect is strong so that the incoherent self energy contribution is less important and only causes minor

quantitative corrections.

Despite the simple BCS form of the self energy, Eq. (7), our result does include the contributions of pairing fluctuations, as in Eq. (4c). It is the simplification via Eq. (5) that encapsulates the fluctuations into a single parameter, Δ_{pg}, via an integration of the fluctuation spectrum, as given in Eq. (6).

3.3 Extended to Fermi gases in a trap

When placed in a 3D isotropic harmonic trap, with a trapping potential $V(r) = \frac{1}{2}m\omega^2 r^2$, one can resort to the local density approximation (LDA), by imposing a local chemical potential $\mu(r) = \mu - V(r)$ and the total particle number constraint,

$$N = \int \mathrm{d}^3 r\, n(r) \tag{19}$$

where $n(r)$ is the local number density, and $\mu \equiv \mu_0 = \mu(0)$ is the chemical potential at the trap center, often referred to as the global chemical potential. Note that here the trap potential does not necessarily have to be isotropic; it may be anisotropic with a variable aspect ratio, including the quasi-2D pancake or quasi-1D cigar shapes as the limit of a large aspect ratio. It may also be an optical lattice, which we shall not cover in this review.

With LDA, at any given location, the fermions are subject to pairing. Below T_c, there exists a superfluid core in the center of the trap. Outside the core, the fermions may or may not be paired, depending on their concrete radial position and the strength of the pairing interaction. When the pairing correlation is strong, one expects to find a pseudogap in the outskirt of the superfluid core. Inside the superfluid core, the fermions locally satisfy the gap equation as well as the pseudogap equation, while the local chemical potential $\mu(r)$ determines the local density $n(r)$. Outside the superfluid core, the fermions are in the normal state, so that the effective pair chemical potential μ_{pair} becomes nonzero. In this case, we need to use the extended gap equation (18) in place of equation (10). As mentioned earlier, the use of the extended gap equation (18) should be restricted to a temperature regime not far above T_c. In the trapped case, this translates into a narrow shell outside the superfluid core. Nevertheless, as the density gets lower towards the trap edge, the gap becomes small and the error introduced into the total number N via the local $n(r)$ is negligible. Thus in our actual numerical calculations, we apply Eq. (18) for the entire shell of Fermi gases outside the superfluid core, and switch to unpaired normal Fermi gas state when the gap becomes tiny, e.g., when $\Delta < 10^{-5}$.

3.4 Thermodynamics and superfluid density

The pseudogap and finite momentum pair excitations necessarily affect the thermodynamic behavior and transport properties, such as the superfluid density. Away from the BCS regime, both Bogoliubov quasiparticles and finite momentum pairs are present at finite T. They serve to destroy the superfluid density and contribute to the entropy. Knowing the excitation spectra, it is straightforward to write down the entropy S, as a sum of fermionic (S_f) and bosonic (S_b) contributions. In a trap, the total entropy involves an integral over the trap, given by $S = \int \mathrm{d}^3 r\, s(r)$ (and similarly for S_f and S_b), where

$$\begin{aligned} s &= s_f + s_b \\ s_f &= -2\sum_{\boldsymbol{k}} [f_k \ln f_k + (1-f_k)\ln(1-f_k)] \\ s_b &= -\sum_{q\neq 0} [b_q \ln b_q - (1+b_q)\ln(1+b_q)] \end{aligned} \tag{20}$$

Here $f_k \equiv f(E_{\boldsymbol{k}})$, and $b_q \equiv b(\Omega_{\boldsymbol{q}} - \mu_{\mathrm{pair}})$. The fermion contribution coincides *formally* with the standard BCS result for noninteracting Bogoliubov quasiparticles [although here $\Delta(T_c) \neq 0$]. And the bosonic contribution is given by the expression for non-directly-interacting bosonic pairs with dispersion $\Omega_{\boldsymbol{q}}$, with an effective mass M^* which is not necessarily equal to $2m$. When the chemical potential μ becomes negative, the entropy S becomes dominantly bosonic, since the fermionic part S_f becomes exponentially suppressed.

One can also write down the energy of the Fermi gas, which consists of a fermionic and bosonic part in a similar fashion. Thus, in a trap, the local energy is given by

$$\begin{aligned} E &= \mu n(r) + E_f + E_b \\ E_f &= \sum_K (\mathrm{i}\omega_n + \epsilon_{\boldsymbol{k}} - \mu(r))G(K) \\ &= \sum_{\boldsymbol{k}} [2E_{\boldsymbol{k}} f_k - (E_{\boldsymbol{k}} - \epsilon_{\boldsymbol{k}} + \mu(r))] + \Delta^2 \chi(0) \\ E_b &= \sum_q (\Omega_{\boldsymbol{q}} - \mu_{\mathrm{pair}}) b_q \end{aligned} \tag{21}$$

where the pair susceptibility $\chi(0)$ is given by Eq. (3) at $Q = 0$. One obtains the total energy by integrating Eqs. (21) over the entire trap.

To end this subsection, we present the expression for the superfluid density, which can be derived using the linear response theory with a generalized Ward identity [25, 56, 139]. In a homogeneous case, it is given by

$$\left(\frac{n_s}{m}\right) = \frac{2}{d}\sum_{\mathbf{k}} \frac{\Delta_{sc}^2}{E_{\boldsymbol{k}}^2}\left[\frac{1-2f(E_{\boldsymbol{k}})}{2E_{\boldsymbol{k}}} + f'(E_{\boldsymbol{k}})\right] \times \left[\left(\vec{\nabla}_{\boldsymbol{k}}\xi_{\boldsymbol{k}}\right)^2 \varphi_{\boldsymbol{k}}^2 - \frac{1}{4}(\vec{\nabla}_{\boldsymbol{k}}\xi_{\boldsymbol{k}}^2)\cdot(\vec{\nabla}_{\boldsymbol{k}}\varphi_{\boldsymbol{k}}^2)\right] = \frac{\Delta_{sc}^2}{\Delta^2}\left(\frac{n_s}{m}\right)^{MF} \quad (22)$$

where $d = 3$ is the dimensionality, $f'(x) = \mathrm{d}f(x)/\mathrm{d}x$, and we have kept (n_s/m) as a combination since on a lattice the mass m is not well defined, but the combination is. The *key result* here is the last line in Eq. (22), where $(n_s/m)^{MF}$ is the BCS mean-field expression for (n_s/m), which necessarily persists into the normal state when a pseudogap exists above T_c. It is the prefactor Δ_{sc}^2/Δ^2 that guarantees that there be no Meissner effects above T_c. Indeed, within the present pairing fluctuation theory, the superfluid density vanishes continuously and nicely as T approaches T_c from below, following the T dependence of Δ_{sc}^2 in the vicinity of T_c. A population imbalanced version of Eq. (22) can be found in Ref. [140]. In a trap, all one needs to do is to integrate the local superfluid density $n_s(r)$ over the entire trap, $N_s = \int \mathrm{d}^3 r n_s(r)$.

4 Key results of the present pairing fluctuation theory

In this section, we will present some key results related to the pseudogap phenomena. We first present the results for a dilute two-component 3D Fermi gas with a short range s-wave pairing interaction, which serves to demonstrate the simple physical picture, and will be a basis of comparison for other cases. Next we shall present the main results for the cuprate superconductors, and then quickly switch to results relevant for atomic Fermi gases, which is the main subject of this Review.

4.1 Two-component homogeneous Fermi gases in the 3D continuum

Figure 9 summarizes the main results of the present theory on the behavior of a 3D Fermi gas with a contact potential. Shown are the phase diagram and related quantities, including T_c, T^*, $\mu(T_c)$, $\Delta(0)$, $\Delta(T_c)$, as well as the pair fraction $2n_p/n$ and the effective inverse pair mass m/M^* at T_c. Here the pair formation temperature T^*, as a crossover temperature, is approximated by the mean field solution of T_c. While the T_c curve is close to its mean-field counterpart in the weak coupling BCS regime, a (shaded) pseudogap phase emerges in the intermediate (crossover or unitary) through strong pairing BEC regimes. Along with the BCS–BEC crossover, the

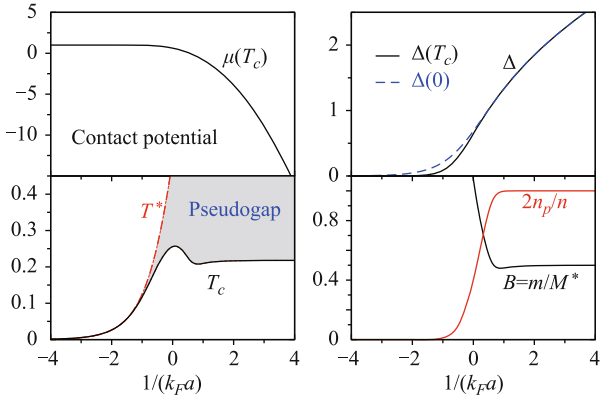

Fig. 9 Calculated phase diagram and T_c, T^*, $\mu(T_c)$, $\Delta(0)$, $\Delta(T_c)$ and pair fraction $2n_p/n$ and inverse pair mass m/M^* (at T_c) of a 3D homogeneous Fermi gas with a contact potential as a function of $1/(k_F a)$. Here n_p denotes the number density of pairs.

fermionic chemical potential μ decreases from E_F in the noninteracting limit, and approaches a large negative given by $-E_b/2$ in the deep BEC regime, where E_b is the two-body binding energy. At the same time, the excitation gaps $\Delta(0)$ and $\Delta(T_c)$, at zero T and T_c, respectively, grow with $1/(k_F a)$. While $\Delta(T_c)$ at T_c roughly vanishes in the BCS regime, it becomes nearly equal to $\Delta(0)$ in the BEC regime. A scrutiny also reveals that the ratio $\Delta/|\mu|$ approaches 0 in the BEC limit, implying that in the deep BEC regime, many-body effects are relatively unimportant so that pairing is dominated by two-body physics. Indeed, the curve of $2n_p/n$ shows that in the BEC regime, essentially all fermions form pairs. A calculation of the pair size reveals that it shrinks in real space with increasing pairing strength [1, 56], leading to a dilute Bose gas of tightly bound fermion pairs in the deep BEC regime.

One feature that seems unique to the present theory is that the T_c curve reaches a maximum near unitarity. At the same time, there is a minimum where μ changes sign. In the BEC limit, T_c approaches its ideal BEC asymptote from below, as expected on physical grounds. This nonmonotonic behavior of T_c can be readily explained. Starting from the intermediate pairing strength regime, the formation of pairs quickly depletes the effective density of fermions, making the effective fermionic density of state decrease, associated with a shrinking Fermi surface. This leads to a decrease in T_c. On the other hand, the bosonic part of the system emerges and grows, as given by the increasing pair density n_p. Beyond the $\mu = 0$ point, the Fermi surface completely vanishes, and n_p reaches its maximum value $n/2$, so that T_c is controlled by the BEC temperature, which increases slowly with m/M^*.

It should be emphasized that, as shown by the m/M^*

curve, except in the deep BEC regime, the effective pair mass differ significantly from $2m$. This should be contrasted with NSR-based theories, which has $M^* = 2m$ in all cases.

As one can see from Fig. 9, in the pseudogap phase, the pseudogap $\Delta(T_c)$ and the pair density n_p grow hand in hand.

Figure 10 illustrates the behavior of the gaps as a function of temperature for a 3D homogeneous Fermi gas at unitarity. The pseudogap at T_c is close to the zero T gap $\Delta(0)$. For weaker coupling toward the BCS limit, the pseudogap $\Delta_{pg}/\Delta(0)$ decreases and vanishes eventually. On the contrary, with increasing pairing strength toward the BEC regime, the ratio $\Delta(T_c)/\Delta(0)$ approaches unity so that the gap becomes essentially temperature independent except at very high T. At low T, following Eq. (16), the pseudogap scales as $\Delta_{pg}(T) \propto T^{3/4}$.

In Fig. 11, we present the typical density of states $N(\omega) = -2\sum_{\boldsymbol{k}} \mathrm{Im}\, G(\omega+\mathrm{i}0, \boldsymbol{k})$ for (a) BEC, (b) BCS and (c) pseudogap regimes for a homogeneous 3D Fermi gas, at different temperatures from slightly above T_c down to $0.5T_c$, half way into the superfluid phase. Note that to distinguish the incoherent pair contributions from that of the condensate to the self energy, we have used a more realistic form of the pseudogap self energy,

$$\Sigma_{pg}(\omega, \boldsymbol{k}) \approx \frac{\Delta_{pg}^2}{\omega + \xi_{\boldsymbol{k}} + \mathrm{i}\gamma} \tag{23}$$

where γ is treated as a phenomenological parameter independent of temperature [141]. The very low but finite DOS for $\omega < 0$ in the BEC regime is purely a consequence of particle-hole mixing due to pairing. Except for the BCS regime, where the gap closes at T_c, a pseudogap is already present at T_c for both the BEC and the pseudogap regimes.

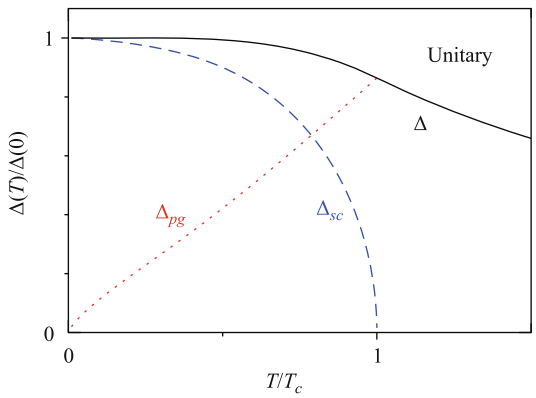

Fig. 10 Normalized gaps as a function of reduced temperature T/T_c at unitarity. The gap at T_c is comparable to the gap at $T = 0$. The curves are calculated for a homogeneous 3D Fermi gas in continuum, with pairing symmetry $\varphi_{\boldsymbol{k}}^2 = 1/[1+(k/k_0)^2]$ at $k_0/k_F = 4$.

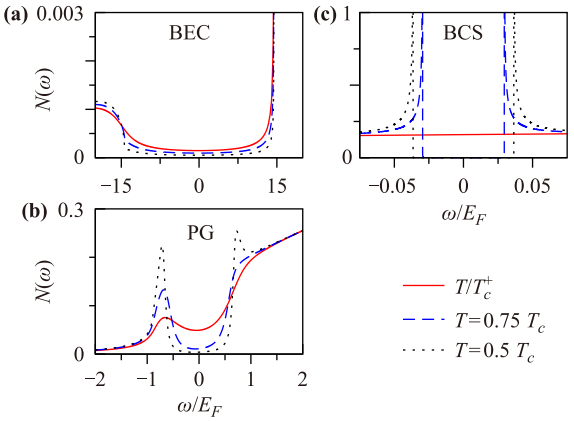

Fig. 11 Fermionic density of states vs energy for the three regimes at three indicated temperatures from slightly above T_c down to the superfluid phase. Note the big difference in the scales. Reproduced from Ref. [126].

From Fig. 11, one can easily conclude that unless one has a very high resolution in experiment, one can no longer use the opening of a gap in the DOS as a signature of superfluid transition in the presence of a pseudogap. Instead, it is a signature of pairing which in general takes place before superfluid phase coherence sets in. This is a very important effect of the pseudogap.

Shown in Fig. 12 is the normalized superfluid density n_s/n in a 3D homogeneous Fermi gas as a function of the reduced temperature T/T_c, for different pairing strengths $U/U_c = 0.7$, 1.0, and 1.5, corresponding to the BCS, unitary, and BEC regimes, respectively. In comparison with the exponential T dependence of the BCS case (black solid curve), a clear deviation can be seen in the unitary case (blue dashed curve) already. This is due to the bosonic pair excitations, which obey the $T^{3/2}$ power law at low T. In the BEC regime (red dot-dashed curve), the

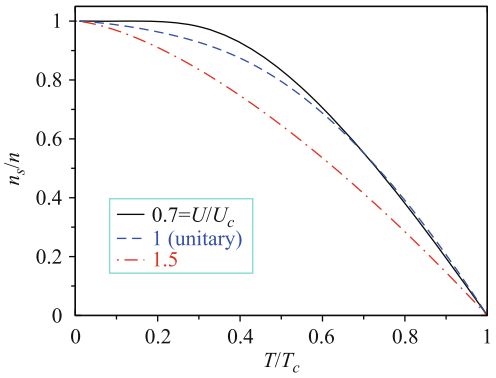

Fig. 12 Normalized superfluid density n_s/n of a 3D homogeneous Fermi gas as a function of T/T_c for three different regimes. Here $U/U_c = 1$ is equivalent to $1/(k_F a) = 0$, the unitary limit. The pseudogap or finite momentum pairs contribute a $T^{3/2}$ power law to the low T dependence, which becomes dominant as U/U_c increases. The calculation was done for an NSR type of potential, $\varphi_{\boldsymbol{k}}^2 = 1/[1 + (k/k_0)^2]$ with $k_0/k_F = 4$.

low T behavior is dominated by the $T^{3/2}$ power law of the bosonic excitations. Indeed, in the BEC regime, fermionic quasiparticles are essentially absent below T_c, due to the large negative chemical potential μ.

Figure 12 confirms that in our theory, due to the generalized Ward identity [25], Meissner effect is necessarily absent above T_c. In this way, our superfluid density vanishes nicely at T_c, unlike some competing scenarios (see, e.g., theories based on NSR) which predicts a first order jump or nonmonotonic temperature dependence at T_c [117, 121, 142, 143].

4.2 Application for the cuprates: Quasi-2D superconductors on a lattice with a d-wave pairing symmetry

When the pairing fluctuation theory is applied to a quasi-2D lattice, it turns out that the lattice periodicity and the low dimensionality bear important consequences. The periodic lattice imposes an upper cut-off in the momentum space, and fermion pairs have to move via virtual ionization. As a result, the superfluid transition temperature T_c scales as $t_{//}^2/U$ at low densities, where $t_{//}$ is the in-plane nearest neighbor hopping integral, and U is the on-site attractive (pairing) interaction. At high densities, calculations show that T_c vanishes abruptly at an intermediate pairing strength so that the BEC regime is not accessible. For high T_c superconductors, the d-wave pairing symmetry further restricts the lower bound of the pair size to that of a unit cell. Along with the non-local effect [144] of the d-wave pairing, the system is essentially always in the high density regime so that T_c vanishes abruptly at an intermediate pairing strength. The high density strongly suppresses the motion of the (finite size) pairs so that at certain point, the pairing strength is so strong that the pairs become localized, with a diverging effective mass $M^* \to \infty$. More details regarding the lattice, low dimensionality and d-wave effects may be found in Ref. [24].

Shown in Fig. 13 are the T_c curves for a d-wave superconductor on a quasi-2D square lattice at relatively high densities relevant to the cuprate superconductors. For all three densities, $T_c/(4t_{//})$ shuts off around 2.2. The chemical potential shown in the inset reveals that the system is still deep in the fermionic regime when T_c vanishes abruptly. The Δ_{pg} curves show that the pseudogap effect is strong. More details regarding the lattice, low dimensionality and d-wave effects may be found in Ref. [24].

In Fig. 14, we present the theoretical cuprate phase diagram calculated using this theory (lines) and compare with experimental data (symbols) in the left panel. In our calculations, we take U to be doping independent,

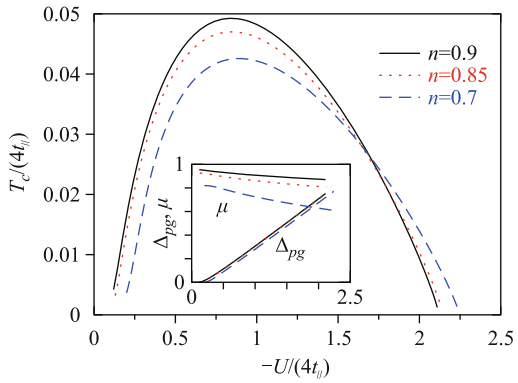

Fig. 13 Superfluid transition temperature T_c as a function of $-U/(4t_{//})$ for fermions on a quasi-2D square lattice, with a d-wave pairing symmetry, at density $n = 0.9$ (*black solid line*), 0.85 (*red dotted*), and 0.7 (*blue dashed line*). Shown in the inset are corresponding $\Delta(T_c)$ and μ. The system is deep in the fermionic regime when T_c vanishes, where the chemical potential μ is not far from its noninteracting value. Here $t_\perp/t_{//} = 0.01$. Reproduced from Ref. [24].

and incorporate the effect of the Mott transition at half filling, by introducing a doping concentration x dependence into the in-plane hopping matrix elements $t_{//} = t_0 x$, as would be expected in the limit of strong on-site Coulomb interactions in a Hubbard model [146]. Therefore, except the weak logarithmic dependence [24] of T_c on the anisotropy $t_\perp/t_{//}$, there is only one free parameter, i.e., U/t_0. Without further tweaking details such as next nearest neighbor hopping t', the agreement between theory and experiment in terms of low T gap $\Delta(0)$, T^* and T_c is remarkable. A later collection of pseudogap at and above T_c are shown in the right panel, which is so scaled that a direct comparison can be made by overlaying it on top of the left panel. Note that the experimental T_c data points in both panels fit the same empirical formula $T_c = T_c^{\max}[1-82.6(0.16-x)^2]$ fairly well [145, 147].

This remarkable (semi-)quantitative agreement between theory and experiment really distinguishes the present theory from other rival theories of high T_c superconductivity. Despite the fact many different high T_c theories have been proposed, one finds it awkward that it is hard to find a high T_c theory that is capable of quantitative computations.

4.3 3D Fermi gas in an isotropic trap

When the typical pair size or coherence length is far smaller than the trap size (more precisely, the size of the Fermi gas cloud), LDA is a good approximation. In Fig. 15, we present the solution of T_c under LDA as a function of $1/(k_F a)$ for a Fermi gas in a 3D isotropic harmonic trap with a contact potential. With no surprise, a pseudogap is found to emerge as the pairing strength

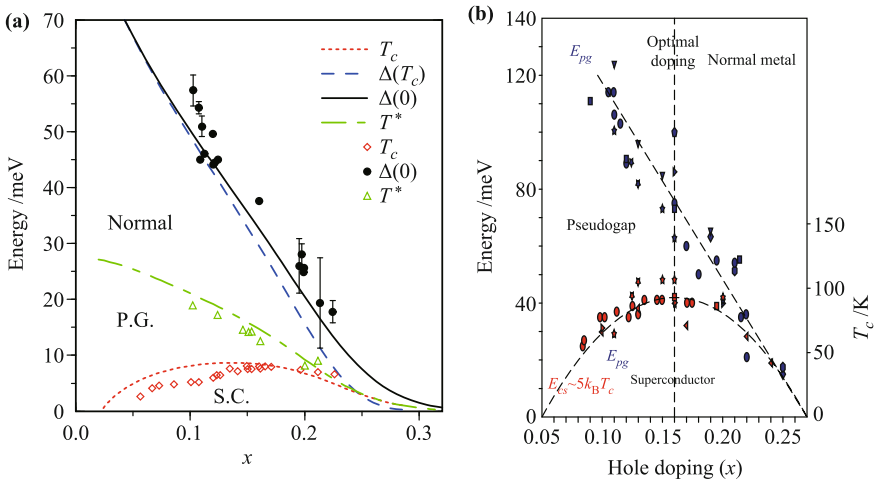

Fig. 14 **(a)** Cuprate phase diagram, reproduced from Ref. [56], showing $\Delta(0)$, T_c, $\Delta(T_c)$, and T^*, calculated for $-U/(4t_0) = 0.047$, and $t_\perp/t_{//} = 0.003$. Shown as symbols are experimental data. The normal, pseudogap, and superconducting phases are labeled with "Normal", "P.G.", and "S.C.", respectively. **(b)** Plot of a recent collection of experimentally measured pseudogap data (with $E_{pg} = 2\Delta_{pg}$, *blue symbols*), reproduced from Ref. [145]. The right axis shows the temperature scales (for T_c and T^*). Note that the right panel has been horizontally squeezed so that it can be overlaid on top of the left panel in the range of $x = 0.05$–0.27. These experimental pseudogap data in the right panel agree with the blue dashed curve for $\Delta_{pg} = \Delta(T_c)$ in the left panel very well.

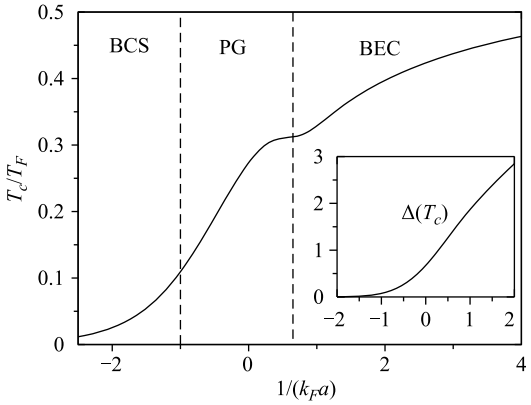

Fig. 15 Behavior of T_c as a function of $1/(k_Fa)$ for a Fermi gas in a 3D isotropic harmonic trap with a short range potential. The plateau is clearly a residue of the maximum-minimum feature in the T_c curve of the homogeneous Fermi gas. As $1/(k_Fa) \to +\infty$, T_c approaches its BEC asymptote in a trap, $0.518T_F$, where T_F is the global Fermi temperature in the noninteracting limit. The inset shows the behavior of corresponding $\Delta(T_c)$. Here "PG" denotes pseudogap.

grows. The behavior of the pseudogap at T_c is shown in the inset. Near unitarity, the plateau in the T_c curve is clearly a residue of the maximum–minimum feature in the T_c curve of the homogeneous Fermi gas. Meanwhile, due to the shrunk cloud size and thus increased density at the trap center in the BEC regime, T_c approaches a much greater BEC asymptote in a trap, $0.518T_F$, as $1/(k_Fa) \to +\infty$, as compared to its homogeneous counterpart, $0.218T_F$. Note that in a trap the global T_F is defined by the Fermi temperature in the noninteracting limit. While the Fermi gas locally satisfies the gas equation as if it were in a homogeneous case, it is easy to conclude that from the weak coupling BCS limit through the deep BEC limit, the central density $n(0)$ is enhanced by a factor of $(0.518/0.218)^{3/2} = 3.66$ by the pairing interaction. (Here we have made use of the relation $E_F \propto n^{2/3}$ for a homogeneous Fermi gas).

Shown in Fig. 16 is the evolution of the spatial density and gap profiles in the 3D harmonic trap as a function of the pairing strength. For illustration purpose, it suffices to focus in the near-BCS through near BEC regimes, without going to the extreme BCS or BEC limits. Indeed, it is the crossover or unitary regime, where the scattering length becomes large, that has been the focus of most studies. In the weak coupling limit, the scattering length is proportional to the interaction strength. For this reason, the unitary regime has often been referred to (mainly by the AMO community) as "strongly interacting". As can be seen from the figure, as the pairing strength increases, the Fermi gas cloud shrinks toward the trap center (upper panel), where the density necessarily increases as a result. At the same time, the spatial distribution of the pairing gap (lower panel) also becomes more focused at the trap center, despite its growing with the pairing strength.

To distinguish the present theory from competing theories, it is worth mentioning that the density profiles are smooth spatially, and evolve monotonically with temperature. This should be contrasted with the theory of Strinati and coworkers [116], which predicts non-monotonic radial dependence and non-monotonic temperature dependence.

It should also mentioned that mean-field calculations

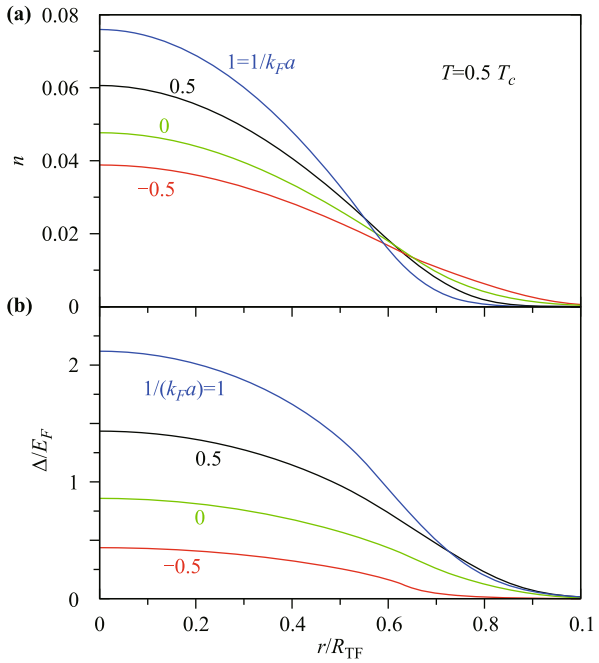

Fig. 16 **(a)** Density and **(b)** gap profile of a Fermi gas in a 3D harmonic trap for various pairing strengths from (near-) BCS to BEC, as labeled. All curves are calculated half way below their corresponding T_c. Here $R_{\rm TF}$ is the Thomas–Fermi (TF) radius, given by the zero T radius in the noninteracting limit.

predict as a signature of superfluidity a kink at the edge of the superfluid core in the density profile [148, 149]. Such a kink is absent in our theory as well as experimental observations. Indeed, it can be easily shown that [56]

$$\begin{aligned} n &= 2Z\Delta^2 + 2\sum_{\boldsymbol{k}} f(\xi_{\boldsymbol{k}}) \\ &= 2Z\Delta_{sc}^2 + 2Z\Delta_{pg}^2 + 2\sum_{\boldsymbol{k}} f(\xi_{\boldsymbol{k}}) \\ &\equiv 2n_c + 2n_p + n_f \end{aligned} \tag{24}$$

where $n_c \equiv Z\Delta_{sc}^2$ is the number density of condensed Cooper pairs [150], $n_f \equiv 2\sum_{\boldsymbol{k}} f(\epsilon_{\boldsymbol{k}} - \mu(r))$ is the density of fermions as though they were free. In Fig. 17, we show the density profile $n(r)$ (black curve) and its component contributions from the condensate $2n_c$ (green), finite momentum pairs $2n_p$ (red) and free fermions n_f (blue), for three representative temperatures $T/T_c = 1$, 0.75, and 0. The right columns show the (de-)composition of the density. At $T/T_c = 0.75$, the density profile is composed of all three components. It is evident that the contribution of finite momentum pairs (red area) is essential in eliminating the kink, which would exist otherwise at the edge of the superfluid core (green area). It is worth mentioning that finite momentum pair density n_p (red curve) is nearly flat inside the superfluid core. This is because $\mu_{\rm pair} = 0$ and the effective pair mass is nearly the same

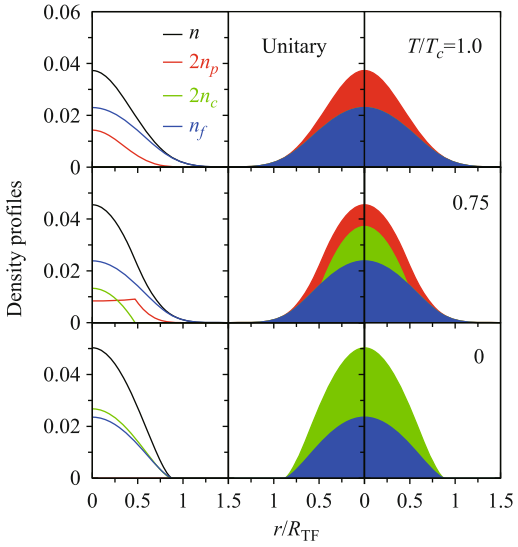

Fig. 17 Decomposition of the density profile $n(r)$ of a Fermi gas in a trap at unitarity for representative temperatures $T/T_c = 1$, 0.75, and 0, as labeled. At T_c, there are only finite momentum pairs (*red*) and fermions (*blue*). Below T_c, the condensate (*green*) develops, and the finite momentum pair contributions decreases. The pair density n_p is nearly uniform inside the superfluid core. At $T = 0$, finite momentum pairs disappear and all pairs are condensed.

across the core. Then n_p starts to decrease gradually outside the core, when $-\mu_{\rm pair}$ acquires a finite value and grows with radius. At T_c, the superfluid core disappears. On the other hand, at $T = 0$, the finite momentum pairs disappear; all pairs are condensed. In the BCS mean-field theory, where $\Delta_{pg} = 0$ and the fermion propagator contains no self energy feedback, Eq. (24) reduces to $n = 2n_c + n_f$. In fact, this is how the density was decomposed in Refs. [148, 149]. Figure 17 shows that without finite momentum pairs, there would be an unphysical kink at the edge of the superfluid core.

Interestingly, it is worth mentioning that under this decomposition, the condensate fraction (green area) $2n_c/n$ is not 100% at $T = 0$ at unitarity since $\mu > 0$, even if the superfluid density is. This result is shown in Fig. 18, where the condensate fraction is plotted as a function of pairing strength for the entire BCS–BEC crossover for a short range potential in both the trapped (black solid) and homogeneous (red dashed line) cases. As one can imagine from Eq. (24), the figure shows that the condensate fraction does not rise to 100% until the BEC regime is reached, where μ changes sign and becomes negative. To understand the small condensate fraction in the BCS regime, one notices that, based on Eq. (24), at zero T this fraction covers the rest part that is not accounted for by the n_f term. Therefore, *it is a measure of the extent to which a fermion lives a life as a component of a Cooper pair rather than an individual fermion.* At unitarity, the

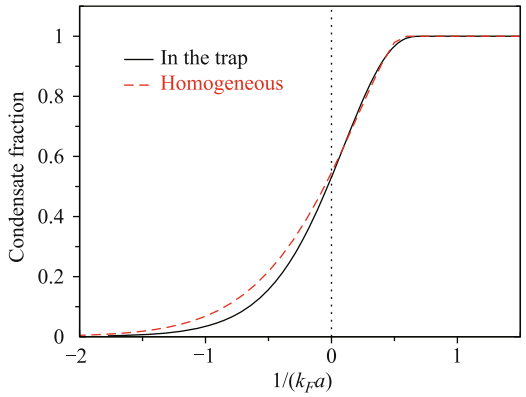

Fig. 18 Condensate fraction at $T = 0$ as a function of $1/k_F a$ in a trapped (*solid line*) and homogeneous (*red dashed line*) Fermi gas with a short-range potential, based on the decomposition given by Eq. (24) and Fig. 17.

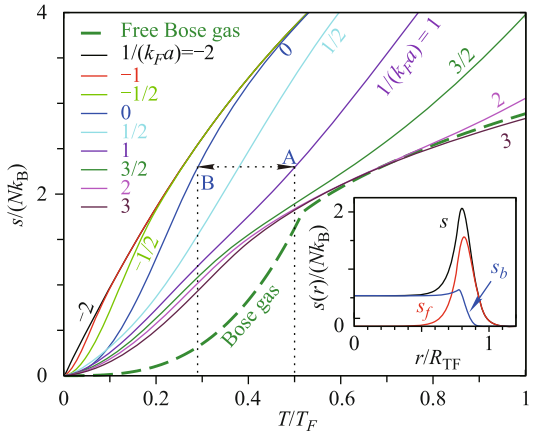

Fig. 19 Entropy per atom as a function of T for different pairing strengths from weak coupling BCS through strong coupling BEC in a harmonic trap. The dotted lines show an isentropic magnetic field sweep between $1/(k_F a) = 1$ and unitarity. For comparison, the dashed line represents the ideal Bose gas. The inset plots the spatial profile of total entropy $s(r)$ (*black curve*) and its fermionic (s_f, *red*) and bosonic (s_b, *blue*) component contributions at unitarity for $T = T_c/4$. Here $T_c = 0.27T_F$. Reproduced from Ref. [153].

condensate fraction is about 0.55 in the homogeneous case, and 0.53 in the trap, respectively. These numbers are close to that from quantum Monte Carlo simulations [151], 0.57 for a total particle number $N = 66$.

The effects of a pseudogap or finite momentum pair contributions on thermodynamics is summarized by Fig. 19, where the entropy per particle is shown for a series of pairing strengths from BCS through BEC for a Fermi gas in a trap [152]. The black curve for $1/(k_F a) = -2$ is close to a noninteracting Fermi gas, exhibiting a linear T dependence at low T. In the opposite strong coupling BEC regime, the $1/(k_F a) = 3$ curve is close to the ideal Bose gas curve, above the BEC asymptote for T_c/T_F, 0.518. At high T (but $\ll T^*$), it is easy to guesstimate from the figure that the entropy in the deep BEC regime is given roughly by half that for a free Fermi gas. The existence of finite momentum pairs allows a continuous evolution from the Fermi gas limit through the Bose gas limit, as the pairing strength increases. The presence of the trap inhomogeneity inevitably makes the situation more complicated that its homogeneous counterpart, leading to a power law T dependence at low T for all pairing strengths.

At unitarity, the distributions of the fermionic and bosonic components of the entropy are shown in the inset. At low T in the broken symmetry, superfluid phase, the bosonic contribution $s_b(r)$ (blue curve) is nearly flat inside the superfluid core, and decays outside the core. On the other hand, the fermionic part, $s_f(r)$, comes mainly from the edge of the Fermi gas cloud, where the pairing gap becomes very small. The sum $s(r)$ has a peak at the trap edge as well. Considering the phase space factor r^2 in the trap integral, the behavior of the entropy S at unitarity is dominated by the fermionic component at the trap edge. As the system evolves deep into the BEC regime, the fermionic part becomes negligible so that the bosonic part eventually dominates.

The above thermodynamics behavior has an immediate consequence. It can be used as a thermometry. It is well known that the temperature measurement in a Fermi gas is notoriously difficult. It is essentially impossible to measure the temperature at an arbitrary interaction strength. Measurement of the temperature in a Fermi gas without a population imbalance has been done successfully only in the BCS limit, deep BEC limit and at unitarity. In practice, it is convenient to connect the actual temperature at a given $1/(k_F a)$ with the temperature in the non-interacting limit, using an adiabatic, isentropic magnetic field sweep. In other words, one can use the entropy in place of the temperature. As an example, the dotted lines in Fig. 19 show how to connect the temperatures at $1/(k_F a)$ and at unitarity.

As an application of the above pseudogap related thermometry, in Fig. 20 we plot the theoretically calculated phase diagram of ^{40}K in a trap with an effective temperature $(T/T_F)^0$ measured adiabatically in the non-interacting limit, and compare with the experimental phase diagram from Jin's group [45, 154]. The black and red curves are T_c and the $N_s/N = 0.01$ contour line, respectively. The experimental data show the contour plot of the condensate fraction. Given the large error bar in the data, we note that the overall trend of the experimental contour of $N_0/N = 0.01$ and the theoretical line for $N_s/N = 0.01$ are in good agreement [155]. One may also compare the T_c curve with that shown in Fig. 15 to see directly the difference between T_c/T_F and $(T_c/T_F)^0$ as an effect of the adiabatic isentropic sweep.

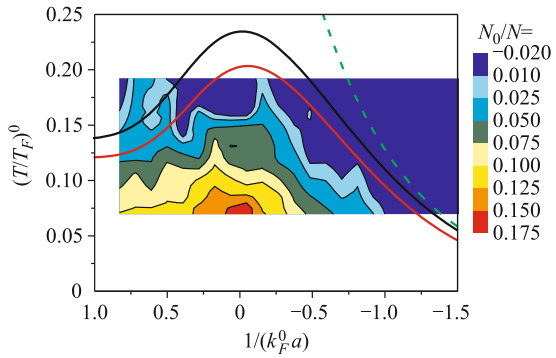

Fig. 20 Phase diagram of ^{40}K. A contour plot of the measured condensate fraction N_0/N as a function of $1/(k_F^0 a)$ and effective temperature $(T/T_F)^0$ in the noninteracting limit is compared with theoretically calculated contour lines at $N_s/N = 0$ (at T_c, *black curve*) and 0.01 (*red curve*). Despite the large uncertainty in experimental data, the overall trend of the experimental contour of $N_0/N = 0.01$ and the theoretical line for $N_s/N = 0.01$ are in good agreement. The dashed line represents the naive BCS result $T_c/T_F^0 \approx 0.615\mathrm{e}^{\pi/(2k_F^0 a)}$. Here $k_F^0 \equiv k_F$ and $T_F^0 \equiv T_F$ are the global Fermi momentum and Fermi temperature, respectively. Reproduced from Ref. [154].

5 Experimental evidence of the pseudogap in atomic Fermi gases

The concept of pseudogap was first introduced into atomic Fermi gases in Ref. [126]. It was not accepted and well understood by the AMO community, until more and more indirect and direct experimental probes provided evidence for its existence. In this section, we shall present evidence of the pseudogap in atomic Fermi gases from various experiments, especially in the unitary regime.

Due to the extreme low T and extreme small size as well as charge neutrality, the choice of experimental probes to ascertain the existence of the pseudogap is very limited for trapped Fermi gases. Typical condensed matter probes such as resistivity measurement, optical conductivity, penetration depth measurement, and angle-resolved photoemission spectroscopy (in the conventional sense) are not available. Therefore, one often has to resort to indirect measurements.

5.1 Thermodynamics and density profiles

Shown in Fig. 21 is the energy per atom for a unitary ^{6}Li Fermi gas. The lines are calculations of the present pairing fluctuation theory, while the symbols are experimental data from the Thomas group [49] at Duke University. The result for noninteracting Fermi gases serves as a calibration of the experimental measurement, where the Thomas–Fermi (TF) approximation works well. It is evident that the theory and experiment agree very well. It is worth mentioning that, in both the noninteracting and unitary cases, a finite trap depth as given by the experiment was used in order to arrive at the good agreement at high T. One of the most important messages one can read off the figure is that the unitary energy curve does not rise to that of the noninteracting curve until $T^* \approx 0.6T_F \gg T_c \approx 0.29T_F$ from the theory. This is a manifestation of the existence of a pseudogap above T_c at unitarity, which helps to lower the energy.

If the energy curve $E(T)$ provides a signature of the pseudogap above T_c at unitarity, the spatial density profile below T_c may serve as *indirect* evidence of the pseudogap below T_c. In Fig. 22 we present a comparison of the one-dimensional density profile $\bar{n}(x) = \int \mathrm{d}z\mathrm{d}y\, n(r)$ of a unitary Fermi gas between theory and experiment, at a temperature substantially below T_c. The agreement is good. There is no sign of the kink behavior at the edge of the superfluid core in the data [157]. We stress that

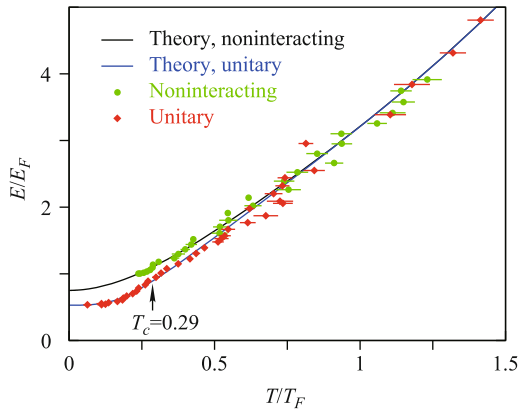

Fig. 21 Comparison between theoretical calculations (lines) and experimental measurements of the energy per atom as a function of T/T_F for noninteracting and unitary ^{6}Li gases. Here the temperature for the unitary case involves a temperature calibration [49]. The unitary and the noninteracting energy data do not merge until about $T^* \approx 0.6T_F$. Reproduced from Ref. [49].

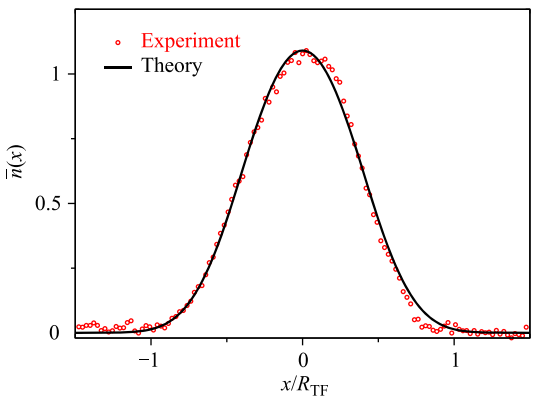

Fig. 22 Comparison between theoretical calculations (*black solid line*) and experimental measurements (*red circles*) of the one-dimensional density profile of a unitary ^{6}Li gas at $T = 0.19T_F \approx 0.7T_c$, in the superfluid phase. Reproduced from Ref. [156].

such a good agreement is not expected for a mean-field theory [148, 149] or a theory that exhibits non-monotonic dependence in radius or temperature [116]. As shown in Fig. 17, the pseudogap or finite momentum pair contributions are essential in arriving at such a smooth density profile.

5.2 Momentum distribution

The presence of a pseudogap necessarily has an important consequence on the momentum distribution N_k of the Fermi gases. Without a pseudogap, N_k would behave very much like a noninteracting Fermi gas at a given temperature. In contrast, it will be spread to a larger range in the momentum space, according to

$$N_{2D}(k) = \int \frac{\mathrm{d}k_z}{2\pi} N_k = \int \frac{\mathrm{d}k_z}{2\pi} \mathrm{d}^3 r\, n_k(r)$$
$$n_k(r) = 1 - \frac{\xi_{\boldsymbol{k}}}{E_{\boldsymbol{k}}} + 2\frac{\xi_{\boldsymbol{k}}}{E_{\boldsymbol{k}}} f(E_{\boldsymbol{k}}) \qquad (25)$$

In Fig. 23, we present the 2D momentum distribution $N_{2D}(k)$ at a series of temperatures from below to far above T_c for different pairing strengths from BCS through (near-)BEC regimes. The left and right columns are from experiment and theory, respectively. The comparison reveals a good agreement between them. The most important message here is that the $N_{2D}(k)$ curves differs significantly for different pairing strengths at $(T/T_F)^0 = 0.3$ and 0.5, above T_c, and they do not merge until $(T/T_F)^0 > 0.7$ where the (pseudo-) excitation gap disappears. Like the $(T/T_F)^0 = 0.11$ case, the difference between the curves for different pairing strengths is caused by the presence of the (pseudo-)gap.

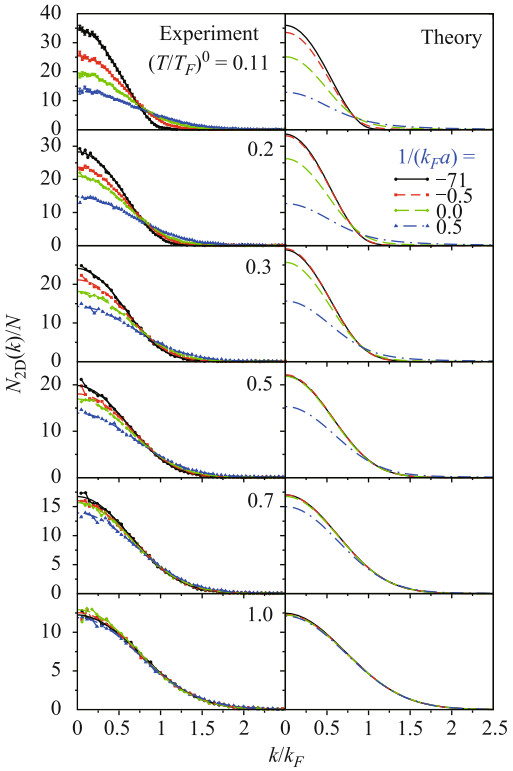

Fig. 23 Temperature evolution of the 2D momentum distribution $N_{2D}(k)$ of a ^{40}K gas in a trap with different pairing strengths from noninteracting through near-BEC cases. The effective temperature in the noninteracting limit, $(T/T_F)^0$, is labeled. Reproduced from Ref. [158].

5.3 (Momentum integrated) radio frequency spectroscopy

Among various experimental techniques, radio-frequency (RF) spectroscopy [47, 160, 161] is arguably the most direct probe for the existence of an excitation gap. The basic physics of a RF process is shown in Fig. 24. Atoms in hyperfine levels 1 and 2 are subject to the pairing interaction, whereas atoms in level 3 are free of such pairing. Therefore, by exciting an atom from level 2 to an unoccupied level 3, one can tell how much extra energy is needed in addition to the hyperfine level splitting. This extra energy, referred to as detuning, provides a measure of the "binding energy" of the level 2 atoms due to interactions. To the lowest order, the RF current is given by

$$I(\nu) = -\frac{1}{2\pi}\sum_{\boldsymbol{k}} A(\boldsymbol{k},\omega) f(\omega)\Big|_{\omega=\xi_{\boldsymbol{k}}-\nu} \qquad (26)$$

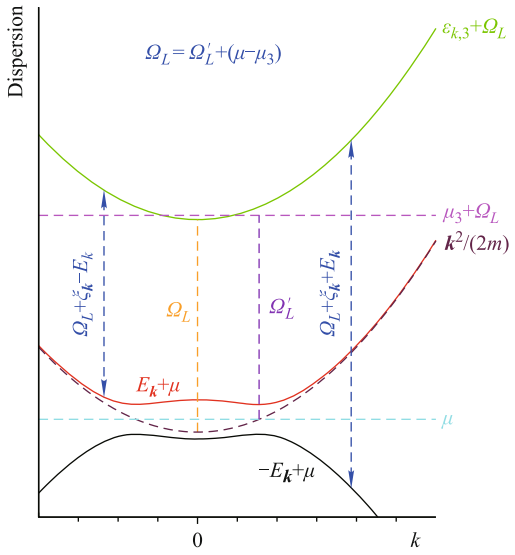

Fig. 24 Energy levels in a RF transition. Ω_L is the RF frequency for exciting a free atom from hyperfine level 2 (*maroon dashed curve*) to level 3 (*green solid curve*). Ω_L' is the same energy but measured relative to the respective chemical potentials. The black and red solid curves are the dispersion of the condensed and thermally excited quasiparticle branches of a paired atom in level 2, with energy level given by $\mp E_{\boldsymbol{k}} + \mu$, respectively. Reproduced from Ref. [159].

where ν is the detuning, $A(\boldsymbol{k},\omega)$ is the spectral function for level 2 atoms, and we have set the RF matrix element to unity. As is well known, when level 2 atoms are paired with level 1 atoms, the spectral function $A(\boldsymbol{k},\omega)$ consists of two branches, the condensed and thermally excited quasiparticle branches, represented in Fig. 24 by the black and red solid curves, respectively. The thermal branch corresponds to negative detuning, and will not be observable for either very low or very high T. The former case will be suppressed by the Fermi function $f(\omega)$, while the high temperature will destroy the pairing in the later case. When interactions exist between level 3 atoms and level 1 atoms, then we have a final state effect, which will also affects the RF spectrum [162–167].

Shown in Fig. 25 is the earliest report on the RF spectroscopy measurement of a unitary ^{6}Li gas at different temperatures. The fractional loss is proportional to $A(\boldsymbol{k},\omega)$ and the RF offset is the detuning ν. The effective temperature T'/T_F, measured in the BEC limit after an isentropic sweep, has been converted to the real temperature T/T_c, using the calculated entropy data shown in Fig. 19. The important feature of this figure is the double peak structure, with one narrow sharp peak at zero detuning, and a broad peak with a positive detuning. The narrow peak can be easily attributed to the transition

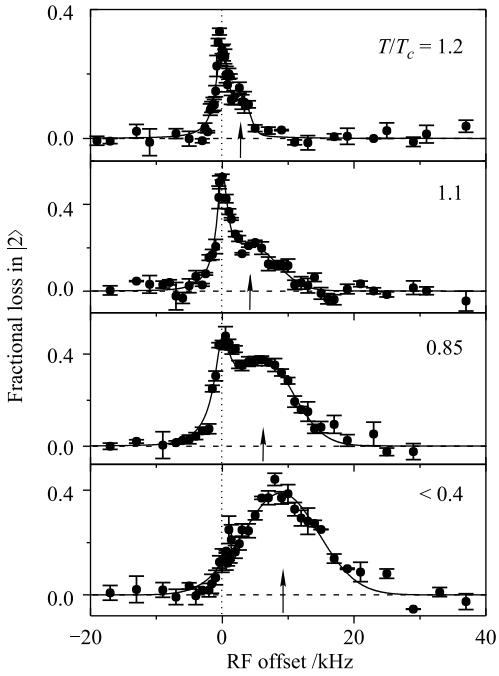

Fig. 25 RF spectra of a unitary ^{6}Li gas for different temperatures. The solid lines are fits to guide the eye. The vertical dotted line marks the atomic transition, and the arrows indicate the peak location of the pairing signal. The original effective temperature T'/T_F has been converted isentropically to the real (reduced) temperature T/T_c using the entropy data shown in Fig. 19. Reproduced from Ref. [47].

from the free level 2 atoms, found at the edge of the trap. On the other hand, the broad peak has been associated with paired level 2 atoms. The trap inhomogeneity necessarily leads to a distribution in the pairing gap, and thus the broadness of the RF signal. The phase space factor r^2 in the trap integral determines that the pairing signal will be peaked at an intermediate radius. At unitarity, for a given gap Δ, the detuning would be a momentum average of

$$\nu = E_{\boldsymbol{k}} + \xi_{\boldsymbol{k}} \geqslant \sqrt{\mu^2 + \Delta^2} - \mu < \Delta \tag{27}$$

with the spectral weight given by the integrand of Eq. (26), namely, the momentum dependent RF current. While quantitatively, the location of the broad pairing peak does not give directly the pairing gap, qualitatively, its presence is a signature of pairing. As revealed by Fig. 25, the broad peak can already be seen above T_c at $T/T_c = 1.2$. The total spectral weight under the broad peak as well as the detuning for this peak increases as T decreases further. Deep in the superfluid phase at $T/T_c < 0.4$, the free atom peak is essentially gone; all level 2 atoms are paired, and the pairing peak detuning reaches its maximum.

Recent experiment [168] and QMC results [169–171] suggest that for ^{6}Li at unitarity, the transition temperature $T_c/T_F \approx 0.17$, substantially lower than 0.29 predicted in the present theory. This further substantiates the existence of a pseudogap above T_c.

The experimental result of Ref. [47] was interpreted successfully [172, 173] using the present pairing fluctuation theory soon after its publication. In Fig. 26, we present a comparison of calculated RF spectra (solid curve, $T_c \approx 0.29T_F$) with experiment (symbols) in a harmonic trap calculated for ^{6}Li at 822 G (on the BEC side of the Feshbach resonance at 834 G) for the two lower experimental temperatures. The overall agreement is satisfactory, which can be further improved by including the final state effect [159]. While our focus remains on qualitative evidence of the pseudogap, we shall not go into details about the final state effect. Interested readers may find further information in Refs. [159, 162, 164–167].

5.4 Momentum resolved radio frequency spectroscopy

Despite the very intuitive picture about the double peak structure in the RF spectra, the momentum integration has caused some disputes regarding the origin of the double peak structure [160, 174], and thus the physical interpretation about the RF spectroscopy measurements. This has a lot to do with the final state effect, first noticed by Müller and coworkers [166]. The lack of simple relation between the pairing gap size and the pairing

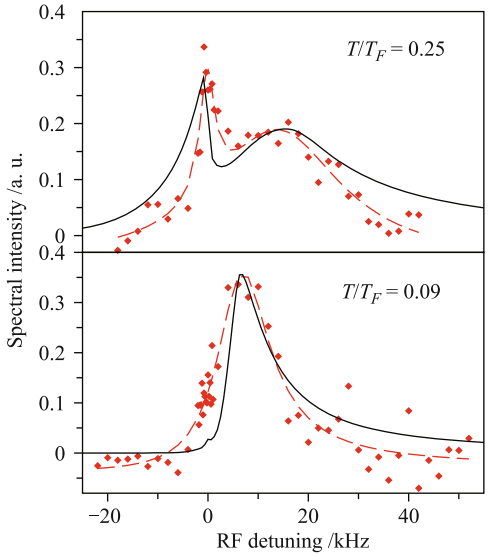

Fig. 26 Comparison of calculated RF spectra (*solid curves*, $T_c \approx 0.29T_F$) with experiment (*symbols*) in a harmonic trap calculated at 822 G for the two lower temperatures. The temperatures were chosen based on Ref. [47]. The dashed lines are a guide to the eye. Reproduced from Ref. [173].

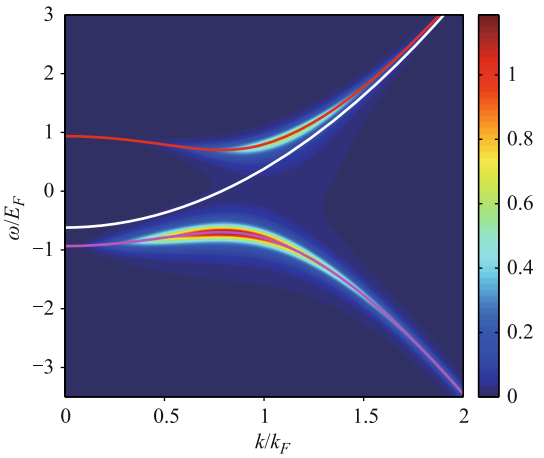

Fig. 27 Contour plots of the occupied spectral intensity at unitarity in a homogeneous Fermi gas for $T/T_c \approx 1.9$. The population of the two branches are determined self-consistently. The white curve represents the dispersion of unpaired atom. Reproduced from Ref. [176].

peak location in the RF spectra has made it difficult to extract the gap from the data quantitatively.

A great step forward was made by Jin and coworkers [175], who performed momentum resolved RF (MRRF) spectroscopy measurement for the first time, in a ^{40}K gas. The RF current is given by the integrand of Eq. (26). It turns out that the MRRF spectroscopy is equivalent to the ARPES [61, 91], which is a very important and useful tool in condensed matter physics. Further simplification comes from the fact that there is no final state effect in a ^{40}K gas. This makes the interpretation of the MRRF spectra relatively simple and unambiguous. In Fig. 27, we present the contour plot of the occupied spectral intensity in the ω–k plane, for a homogeneous 3D Fermi gas at unitarity at $T/T_F = 0.5$. The two branches corresponding to the condensed and thermally excited quasiparticles shown in Fig. 24 are clearly visible. For comparison, the white curve shows the dispersion of a free atom, with the same chemical potential. The particle–hole mixing as a pairing effect is evident, as manifested by the avoided crossing and back-bending of both the lower and upper branches. This back-bending takes place at $k = \sqrt{2m\mu} < k_F$. To see the upper branch clearly, one needs to have relatively high temperature which is comparable with Δ.

Ideally, one would like to have a homogeneous system. Unfortunately, a trap potential is necessary in order to hold the Fermi gas together. This complicates the otherwise very simple interpretation of the RF spectra.

In Fig. 28, we present a comparison of the key result on the spectral intensity map between experiment (left) and theory (right) for a unitary Fermi gas above T_c at $T/T_c = 1.1$. The similarity between the two panels is obvious. As can be seen, a large fraction of the spectral weight has been shifted from the free atom branch to the paired atom branch. Indeed, at high T where pairing effect is negligible, the spectral weight concentrates on the free particle dispersion (not shown). As the temperature decreases, a second (downward dispersing) branch emerges. This lower branch is associated with the breaking of a pair and necessarily contains trap averaging effects. With decreasing temperature, the intensity map first bifurcates and eventually at very low T becomes dominated by the lower branch, when essentially all atoms are paired.

From Fig. 28, such bifurcation and downward dispersion already take place above T_c, indicating unambiguously that a pseudogap exists in the unitary Fermi gas. To extract this downward dispersion, the energy distribution curves (EDCs) have been fitted to a single Gaussian function experimentally. This leads to the white dashed curve in the right panel. The white solid dispersion curve is obtained theoretically following the same procedure. A BCS-like fit to this dispersion can be used to determine the pairing gap, as has been done in Ref. [175], as $E_s = \mu - \sqrt{\xi_{\boldsymbol{k}}^2 + \Delta^2}$. The best fit to the experimental dispersion yields $\Delta = 9.5$ kHz, comparable to E_F. The agreement between experiment and theory is reasonably good, despite the trap inhomogeneity. The white dashed experimental curve back bends at $k > k_F$, in contradiction to what is expected on physical ground at unitarity. This is mainly caused by the low experimental resolution and the incorrect single-Gaussian function fitting procedure. Our theory predicts double peaks in

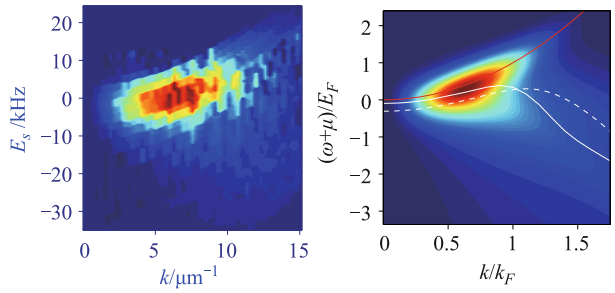

Fig. 28 Comparison between experiment **(left)** and theory **(right)** of the contour plots of the occupied spectral intensity in a unitary Fermi gas in a trap at $T/T_c \approx 1.1$. The red curve represents the free atom dispersion. A large amount of spectral weight has been shifted from a free atom peak to a paired atom peak (downward dispersing curve). Here the intensity increases from dark blue for 0 to dark red for the maximum, and the solid and dashed white lines indicate the loci of the peaks in the energy distribution curves from theory and experiment, respectively. The single particle energy E_s is equivalent to $\omega + \mu$, the energy measured relative to the bottom of the band. Reproduced from Refs. [175, 176].

the EDC curves for $k \geqslant k_F$, and this has been confirmed by careful inspection of the experimental data [176]. Further improved experimental data [177] have led to a dispersion much closer to the theoretical result. The observation of a pseudogap has also been confirmed by Ref. [178, 179].

It should be mentioned that via the simple approximation Eq. (5), the present pairing fluctuation theory has demonstrated in a simple, analytic way that a pseudogap necessarily exists when the pairing interaction is strong. For NSR-based theories, due to the inconsistency between the gap equation, which contains no pairing fluctuation contributions, and the number equation, one would have to extract the pseudogap from the renormalized spectral function in a cumbersome way. In this sense, the numerical route of Strinati *et al.* [180, 181] can be viewed simply as a confirmation of our analytically result.

5.5 Population imbalanced Fermi gases

In this subsection, we provide evidence for the existence of a pseudogap in population imbalanced Fermi gases. For extension of the present pairing fluctuation theory to the case of population imbalance, we refer the readers to Refs. [132–134].

Shown in Fig. 29 is the calculated phase diagram of a population imbalanced Fermi gas in a trap at unitarity. The overall polarization, $p = (N_\uparrow - N_\downarrow)/N$, is different from its local counterpart. At low T, phase separation (PS) takes place, where a BCS superfluid core of an equal spin mixture at the trap center is surrounded by polarized Fermi gases. Above the PS phase, there exist intermediate temperature superfluids, which is referred

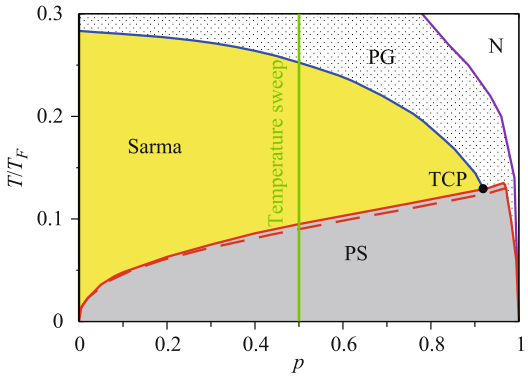

Fig. 29 Calculated phase diagram of a population imbalanced Fermi gas in a trap at unitarity. Here "PS" stands for phase separation, "Sarma" for polarized Sarma superfluid, "PG" for pseudogapped normal state, "N" for unpaired normal state, and "TCP" for tricritical point. Reproduced from Ref. [133].

to as Sarma superfluid, for which the local spin polarization penetrates all the way into the trap center. Above the Sarma phase, there is a pseudogap phase (PG) where pseudogap exists without superfluidity, before the system becomes unpaired normal state (N) at high T.

The behavior of the polarization at the trap center, $(n_\uparrow - n_\downarrow)/n_\uparrow(T = 0)$, in a temperature sweep at $p = 0.5$, is shown in the upper panel of Fig. 30. An important feature here is that its evolution across T_c is smooth, without a clear signature of the superfluid transition. A downturn is predicted at the crossover temperature T^*, where the pseudogap becomes negligible. We emphasize that this smooth evolution across T_c is a consequence of the fact that the total excitation gap is continuous across T_c. This feature has been verified by experimental data from the Ketterle group [182], as shown in the lower panel. Note that the experimental trap depth is proportional to the temperature. The agreement between experiment and theory is remarkable. Therefore, we conclude that the experimental data have provided strong support for the existence of a pseudogap above T_c.

5.6 Dispute against the existence of a pseudogap

Despite the definitive evidence of the pseudogap from various experiments, especially the MRRF spectroscopy measurements, there have still been some disputes against the existence of the pseudogap from thermodynamics measurement [183, 184]. Especially, in Ref. [183], Salomon and coworkers reported "a T^2 dependence of the pressure with temperature", and thus claimed that "This behavior is reminiscent of a Fermi liquid, and indicates that pseudogap effects expected for strongly interacting Fermi superfluids do not show up at the thermodynamic level within our experimental precision." *However, this cannot be used as evidence against the*

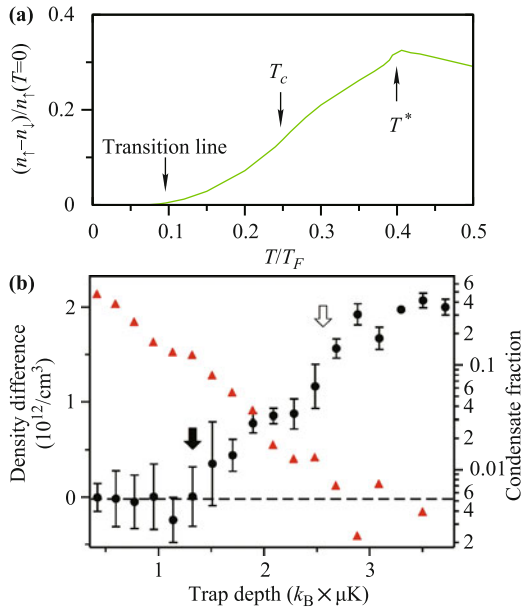

Fig. 30 **(a)** Relative density difference at the trap center at low T as a function of T/T_F at $p = 0.5$, i.e., along the vertical green line in Fig. 29. The three arrows indicate the PS/Sarma boundary, the Sarma superfluid/PG transition T_c, and the PG/N crossover temperature T^*, respectively. **(b)** Experimental data from MIT, showing the density difference (*black solid circles*, left axis) at the trap center of a unitary Fermi gas at $p = 0.5$, along with the condensate fraction (*red triangles*, right axis), as a function of trap depth, which is proportional to T. The solid and empty arrows indicate the PS/Sarma transition temperature and superfluid T_c, respectively. Reproduced from Refs. [133, 182].

existence of a pseudogap, because the macroscopic quantity pressure used in their equation of state (EOS) involves a trap and momentum integration over all microscopic states. There are many possible microscopic states which can produce the same macroscopic thermodynamic quantities after integration. This is a many-to-one mapping. For example, within the BCS mean-field theory, the relation between pressure and energy of a Fermi gas with a contact potential at unitarity is given by $p/E = 2/3$, exactly the same as that for a noninteracting Fermi gas (which exhibits an ideal Fermi liquid behavior). In fact, their key experimental data were taken at $(T/\mu)^2 > 0.1$, or equivalently, $T/\mu > 0.3$. This is far from being a low T regime, where one can talk about power law dependence. At such a high temperature, it is not particularly useful to extract its power law dependence on T. The pressure calculated with a pseudogap would follow a similar T dependence in this temperature regime, just like that of the energy (per particle), $E(T)$.

6 Where to look further for the pseudogap

6.1 Effects of particle–hole fluctuations

As in most other theories of BCS–BEC crossover, e.g., the NSR-based theories, the particle–hole channel has been dropped in the treatment of the present pairing fluctuation theory. This is justified in the context of superconductivity, where the particle–hole channel mainly contributes to a change in the chemical potential, which can be taken from experiment. In addition, superfluidity and pairing concerns primarily the particle–particle channel. In many cases, the pairing interaction strength is not precisely known, and thus may be treated as a fitting parameter. Nevertheless, when the pairing interaction strength is indeed known precisely, one may need to consider the effect of particle–hole fluctuations.

In the weak coupling limit, the contribution of particle-hole fluctuations was first considered by Gor'kov and Melik-Barkhudarov (GMB) [185] to the leading order. They found that both T_c and zero temperature gap are suppressed by a *big* factor of $(4e)^{1/3} \approx 2.22$. A few others have recently considered particle–hole fluctuations within the context of Fermi gases and BCS–BEC crossover [186–189]. In Ref. [190], the present pairing fluctuation theory is extended to include the particle–hole channel in such a fashion that the T-matrices of both the particle–particle channel and the particle–hole channel intertwine with each other and are treated self-consistently. The main result is that in the BCS through unitary regime where the chemical potential $\mu > 0$, particle–hole fluctuations cause an effective reduction of the pairing strength. In particular, the unitary limit is shifted towards the BEC regime, to $1/(k_F a) \approx 0.35$. The original maximum T_c at unitarity (see Fig. 9) has now occurred at the new location. This seems to be in good agreement with the QMC result from Ref. [170], which reported a maximum $T_c/E_F \approx 0.25$ around $1/(k_F a) = 0.47$. Depending how the interaction parameter is determined, this seems to suggest that one may need to consider looking for the pseudogap around the new unitary limit in future experiments. Further details of the effect of particle–hole fluctuations may be found in Ref. [190].

6.2 Widespread pseudogap phenomena

There are widespread pseudogap related phenomena in ultracold Fermi gases. In this section, we shall only name a few examples, instead of giving a full search.

For a wide Feshbach resonance such as the widely studied resonances in ^{6}Li and ^{40}K, the closed channel fraction has turned out to be closely related to the pseudogap. In Fig. 31, we show the closed-channel fraction as a function of T for a unitary Fermi gas, calculated using a two-channel version of the present pairing fluctuation theory [191]. Here the black (N_{b0}) and red (N_b) curves stand for the condensed and thermal part of the closed-channel

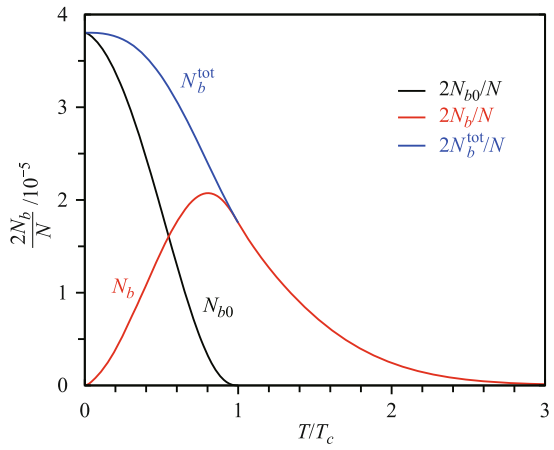

Fig. 31 Closed-channel fraction as a function of T/T_c at unitarity for $T_F = 0.4$ μK for ^{6}Li in a harmonic trap. The black, red, and blue curves are the condensed ($2N_{b0}/N$), noncondensed ($2N_b/N$) and total ($2N_b^{\rm tot}/N$) fractions, respectively. Here $T_c = 0.273T_F$. Reproduced from Ref. [191].

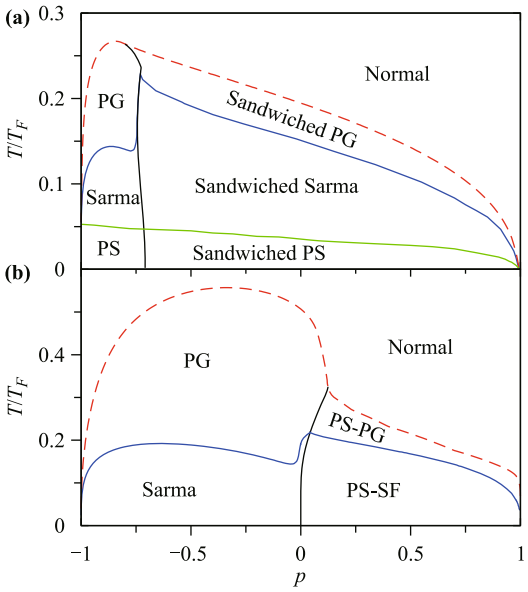

Fig. 32 T–p phase diagram of a ^{6}Li–^{40}K mixture in a harmonic trap at **(a)** unitarity and **(b)** $1/(k_Fa) = 0.5$, with $\omega_\uparrow = \omega_\downarrow$. The solid lines separate different phases, and the (red) dashed line is approximated by mean field calculations. We choose the population imbalance $p > 0$ when ^{40}K is the majority. Here "PG" and "PS" indicate pseudogapped normal state and phase separation, respectively, and "SF" stands for superfluid. The PS-PG and PS-SF phase has an "inverted" two-shell structure, with a normal gas of the majority heavy atoms at the trap center, surrounded by a superfluid or pseudogapped paired Fermi–Fermi mixture. Reproduced from Ref. [135].

molecules, while the blue curve ($N_b^{\rm tot}$) stands for the sum. They are proportional to Δ_{sc}^2, Δ_{pg}^2, and Δ^2, respectively. At low T, the calculated fraction $2N_b^{\rm tot}/N$ as a function of pairing strength is in good quantitative agreement with experiment [191, 192]. It is known that at unitarity, pairing can exist only due to many-body effect. Above T_c, should there be no pairing (or equivalently, pseudogap), the closed-channel fraction would drop to zero due to the inter-channel coupling. Therefore, detection of the closed-channel fraction above T_c should provide a direct measurement of the pseudogap.

The pseudogap phenomena can be found not only in equal mass two component Fermi gases, but also in a Fermi–Fermi mixture, with a strong mass imbalance. In Fig. 32, we present a phase diagram for a ^{6}Li–^{40}K mixture in a harmonic trap (a) at unitarity and (b) in the near-BEC regime $1/(k_Fa) = 0.5$, with $\omega_\uparrow = \omega_\downarrow$. Here ω_σ is the angular frequency of the spin dependent trapping potential. The convention is such that $p > 0$ when the heavy species is the majority. The "PS", "Sarma" and "PG" phase in Fig. 32(a) at unitarity is similar to that in Fig. 29. As usual, at the highest temperature, the system behaves like a mix of uncorrelated normal Fermi gases. Otherwise, the dominant part of the phase diagram at unitarity is a sandwiched three-layer shell structure, for which the inner and outer shells are normal Fermi gases, while the mid-shell is either a BCS, Sarma superfluid or a PG normal state, for a temperature from low through high. In the near BEC case in Fig. 32(b), the PS phase for $p < 0$ is no longer stable and the PG and Sarma regions expands substantially. For $p > 0$, the outer shell of a majority Fermi gas has disappeared so that the system becomes an "inverted" two-shell structure, with a majority Fermi gas at the trap center, surrounded by a superfluid or pseudogapped paired Fermi–Fermi mixture in the outer shell. Such two-shell or three-shell structures and the local density profiles may be probed using the *in situ* phase-contrast imaging and 3D image reconstruction technique as in Ref. [182]. One may also use vortex lattices [50] to detect the (sandwiched) PS and Sarma state, so as to distinguish the superfluid and pseudogapped phases. The paired state may also be detected using a Bragg spectroscopy technique [193, 194], which may also be able to distinguish condensed versus noncondensed pairs.

It should be emphasized that the sandwiched PG and the PS-PG phases are both very unusual and very interesting. The associated phase separation involves pseudogapped normal state rather than a superfluid state. Such phase separations have never been predicted or reported before in the literature.

There are many other experiments and physical quantities which exhibit pseudogap phenomena. For example, atomic Fermi gases on optical lattices will be another realm to search for the pseudogap in the future, despite that experiment on optical lattices falls far behind theory. Another realm is 2D Fermi gases, since low dimensionality intrinsically enhances fluctuations, including the pseudogap related pairing fluctuations. It is ex-

pected that more support for the existence of a pseudogap will come up as new experiments become available.

7 Summary

In summary, we have given a review of the study of the pseudogap physics in atomic Fermi gases, and presented a series of experimental evidence of the existence of a pseudogap in Fermi gases, especially in the unitary regime. In this context, we have introduced a pairing fluctuation theory, and have shown that it thus far has addressed successfully multiple atomic Fermi gas experiments. In particular, the momentum resolved radio frequency spectroscopy measurement has provided the most direct probe and the most convincing evidence of the pseudogap. Since the existence of a pseudogap is a natural consequence of the present theory, and most competing theories do not have a pseudogap in their fermion self energy in a self-consistent fashion, the experimental evidence of a pseudogap can be viewed as a strong support for this theory. Given the analogy between superfluidity in Fermi gases and superconductivity in high T_c superconductivity, we argue that the present pairing fluctuation theory for the pseudogap is also a strong candidate for high T_c superconductivity.

Acknowledgements This work was supported by the National Basic Research Program of China (Grant Nos. 2011CB921303 and 2012CB927404), the National Natural Science Foundation of China (Grant Nos. 10974173 and 11274267), and the Natural Science Foundation of Zhejiang Province (Grant No. LZ13A040001).

References and notes

1. Q. J. Chen, J. Stajic, S. N. Tan, and K. Levin, BCS–BEC crossover: From high temperature superconductors to ultracold superfluids, *Phys. Rep.*, 2005, 412(1): 1
2. I. Bloch, J. Dalibard, and W. Zwerger, Many-body physics with ultracold gases, *Rev. Mod. Phys.*, 2008, 80: 885
3. J. M. Maldacena, The large N limit of superconformal field theories and supergravity, *Adv. Theor. Math. Phys.*, 1998, 2: 231, see also: arXiv: hep-th/9711200v3
4. E. Witten, Anti De Sitter space and holography, *Adv. Theor. Math. Phys.*, 1998, 2: 253
5. O. Aharony, S. S. Gubser, J. Maldacena, H. Ooguri, and Y. Oz, Large N field theories, string theory and gravity, *Phys. Rep.*, 2000, 323(3–4): 183
6. M. Čubrović, J. Zaanen, and K. Schalm, String theory, quantum phase transitions, and the emergent Fermi liquid, *Science*, 2009, 325(5939): 439
7. T. Timusk and B. Statt, The pseudogap in high-temperature superconductors: An experimental survey, *Rep. Prog. Phys.*, 1999, 62(1): 61
8. J. R. Schrieffer, Theory of Superconductivity, 3rd Ed., Perseus Books, Reading, MA, 1983
9. S. N. Bose, Plancks gesetz und lichtquantenhypothese, *Z. Phys.*, 1924, 26(1): 178
10. A. Einstein, Quantentheorie des einatomigen idealen gases (II), *Sitzungsberichte der Preussischen Akademie der Wissenschaften*, 1925, 1: 3
11. L. Pitaevskii and S. Stringari, Bose–Einstein Condensation, New York: Oxford, 2003
12. C. J. Pethik and H. Smith, Bose–Einstein Condensation in Dilute Gases, Cambridge: Cambridge University Press, 2002
13. D. M. Eagles, Possible pairing without superconductivity at low carrier concentrations in bulk and thin-film superconducting semiconductors, *Phys. Rev.*, 1969, 186(2): 456
14. A. J. Leggett, Diatomic molecules and cooper pairs, in: Modern Trends in the Theory of Condensed Matter, Berlin: Springer-Verlag, 1980, pp. 13–27
15. P. Nozières and S. Schmitt-Rink, Bose condensation in an attractive fermion gas: From weak to strong coupling superconductivity, *J. Low Temp. Phys.*, 1985, 59(3–4): 195
16. R. Friedberg and T. D. Lee, Boson–Fermion model of superconductivity, *Phys. Lett. A*, 1989, 138(8): 423
17. T. Friedberg and T. D. Lee, Gap energy and long-range order in the boson–fermion model of superconductivity, *Phys. Rev. B*, 1989, 40: 6745
18. C. A. R. Sá de Melo, M. Randeria, and J. R. Engelbrecht, Crossover from BCS to Bose superconductivity: Transition temperature and time-dependent Ginzburg–Landau theory, *Phys. Rev. Lett.*, 1993, 71: 3202
19. M. Randeria, Crossover from BCS theory to Bose-Einstein Condensation, in: Bose–Einstein Condensation, edited by A. Griffin, D. Snoke, and S. Stringari, Cambridge: Cambridge University Press, 1995, pp. 355–392
20. B. Jankó, J. Maly, and K. Levin, Pseudogap effects induced by resonant pair scattering, *Phys. Rev. B*, 1997, 56(18): R11407(R)
21. J. Maly, B. Jankó, and K. Levin, Numerical studies of the s-wave pseudogap state and related T_c: The "pairing approximation" theory, *Physica C*, 1999, 321(1–2): 113
22. J. Maly, B. Jankó, and K. Levin, Superconductivity from a pseudogapped normal state: A mode-coupling approach to precursor superconductivity, *Phys. Rev. B*, 1999, 59: 1354
23. Q. J. Chen, I. Kosztin, B. Jankó, and K. Levin, Pairing fluctuation theory of superconducting properties in underdoped to overdoped cuprates, *Phys. Rev. Lett.*, 1998, 81: 4708
24. Q. J. Chen, I. Kosztin, B. Jankó, and K. Levin, Superconducting transitions from the pseudogap state: d-wave symmetry, lattice, and low-dimensional effects, *Phys. Rev. B*, 1999, 59: 7083
25. I. Kosztin, Q. J. Chen, B. Jankó, and K. Levin, Relationship between the pseudo- and superconducting gaps: Effects of residual pairing correlations below T_c, *Phys. Rev. B*, 1998, 58: R5936(R)

26. R. Micnas, J. Ranninger, and S. Robaszkiewicz, Superconductivity in narrow-band systems with local nonretarded attractive interactions, *Rev. Mod. Phys.*, 1990, 62: 113
27. R. Micnas and S. Robaszkiewicz, Superconductivity in systems with local attractive interactions, *Cond. Matt. Phys.* (*Lviv*), 1998, 13: 89
28. R. Micnas, M. H. Pedersen, S. Schafroth, T. Schneider, J. J. Rodríguez-Núñez, and H. Beck, Excitation spectrum of the attractive Hubbard model, *Phys. Rev. B*, 1995, 52: 16223
29. J. Ranninger and J. M. Robin, Manifestations of the pseudogap in the boson–fermion model for Bose–Einstein-condensation-driven superconductivity, *Phys. Rev. B*, 1996, 53: R11961(R)
30. M. Drechsler and W. Zwerger, Crossover from BCS-superconductivity to Bose-condensation, *Ann. Phys.*, 1992, 1: 15
31. R. Haussmann, Crossover from BCS superconductivity to Bose–Einstein condensation: A self-consistent theory, *Z. Phys. B*, 1993, 91(3): 291
32. R. Haussmann, Properties of a Fermi liquid at the superfluid transition in the crossover region between BCS superconductivity and Bose–Einstein condensation, *Phys. Rev. B*, 1994, 49: 12975
33. O. Tchernyshyov, Noninteracting Cooper pairs inside a pseudogap, *Phys. Rev. B*, 1997, 56: 3372
34. E. V. Gorbar, V. M. Loktev, and S. G. Sharapov, Crossover from BCS to composite-boson (local-pair) superconductivity in quasi-2D systems, *Physica C*, 1996, 257(3–4): 355
35. V. P. Gusynin, V. M. Loktev, and S. G. Sharapov, Phase diagram of a 2D metal system with a variable number of carriers, *JETP Lett.*, 1997, 65(2): 182
36. M. Marini, F. Pistolesi, and G. C. Strinati, Evolution from BCS superconductivity to Bose condensation: Analytic results for the crossover in three dimensions, *Eur. Phys. J. B*, 1998, 1(2): 151
37. B. DeMarco and D. S. Jin, Onset of Fermi degeneracy in a trapped atomic gas, *Science*, 1999, 285(5434): 1703
38. M. H. Anderson, J. R. Ensher, M. R. Matthews, C. E. Wieman, and E. A. Cornell, Observation of Bose–Einstein condensation in a dilute atomic vapor, *Science*, 1995, 269(5221): 198
39. C. C. Bradley, C. A. Sackett, J. J. Tollett, and R. G. Hulet, Evidence of Bose–Einstein condensation in an atomic gas with attractive interactions, *Phys. Rev. Lett.*, 1995, 75: 1687
40. C. C. Bradley, C. A. Sackett, J. J. Tollett, and R. G. Hulet, Evidence of Bose–Einstein condensation in an atomic gas with attractive interactions [*Phys. Rev. Lett.* 75, 1687 (1995)], *Phys. Rev. Lett.*, 1997, 79: 1170
41. K. B. Davis, M. Mewes, M. R. Andrews, D. S. Durfee, D. M. Kurn, W. Ketterle, and W. Ketterle, Bose–Einstein condensation in a gas of sodium atoms, *Phys. Rev. Lett.*, 1995, 75(22): 3969
42. M. Greiner, C. A. Regal, and D. S. Jin, Emergence of a molecular Bose–Einstein condensate from a Fermi gas, *Nature*, 2003, 426(6966): 537
43. S. Jochim, M. Bartenstein, A. Altmeyer, G. Hendl, S. Riedl, C. Chin, J. H. Denschlag, and R. Grimm, Bose–Einstein condensation of molecules, *Science*, 2003, 302(5653): 2101
44. M. W. Zwierlein, C. A. Stan, C. H. Schunck, S. M. Raupach, S. Gupta, Z. Hadzibabic, and W. Ketterle, Observation of Bose–Einstein condensation of molecules, *Phys. Rev. Lett.*, 2003, 91(25): 250401
45. C. A. Regal, M. Greiner, and D. S. Jin, Observation of resonance condensation of fermionic atom pairs, *Phys. Rev. Lett.*, 2004, 92(4): 040403
46. M. Bartenstein, A. Altmeyer, S. Riedl, S. Jochim, C. Chin, J. H. Denschlag, and R. Grimm, Crossover from a molecular Bose–Einstein condensate to a degenerate Fermi gas, *Phys. Rev. Lett.*, 2004, 92(12): 120401
47. C. Chin, M. Bartenstein, A. Altmeyer, S. Riedl, S. Jochim, J. H. Denschlag, and R. Grimm, Observation of the pairing gap in a strongly interacting Fermi gas, *Science*, 2004, 305(5687): 1128
48. M. W. Zwierlein, C. A. Stan, C. H. Schunck, S. M. Raupach, A. J. Kerman, and W. Ketterle, Condensation of pairs of fermionic atoms near a Feshbach resonance, *Phys. Rev. Lett.*, 2004, 92(12): 120403
49. J. Kinast, A. Turlapov, J. E. Thomas, Q. J. Chen, J. Stajic, and K. Levin, Heat capacity of a strongly interacting Fermi gas, *Science*, 2005, 307(5713): 1296
50. M. W. Zwierlein, J. R. Abo-Shaeer, and A. Schirotzek, and W. Ketterle, Vortices and superfluidity in a strongly interacting Fermi gas, *Nature*, 2005, 435: 1047
51. M. W. Zwierlein, A. Schirotzek, C. H. Schunck, and W. Ketterle, Fermionic superfluidity with imbalanced spin populations, *Science*, 2006, 311(5760): 492
52. G. B. Partridge, W. Li, R. I. Kamar, Y. A. Liao, and R. G. Hulet, Pairing and phase separation in a polarized Fermi gas, *Science*, 2006, 311(5760): 503
53. P. Fulde and R. A. Ferrell, Superconductivity in a strong spin-exchange field, *Phys. Rev.*, 1964, 135(3A): A550
54. A. I. Larkin and Yu. N. Ovchinnikov, Neodnorodnoe sostoyanie sverkhprovodnikov, *Zh. Eksp. Teor. Fiz.*, 1964, 47: 1136
55. I. Larkin and Yu. N. Ovhinnikov, Nonuniform state of superconductors, *Sov. Phys. JETP*, 1965, 20: 762
56. Q. J. Chen, Generalization of BCS theory to short coherence length superconductors: A BCS-Bose-Einstein crossover scenario, Ph.D. thesis, University of Chiago, 2000, available in the ProQuest Dissertations & Theses Database online.
57. Q. J. Chen, J. Stajic, and K. Levin, Applying BCS–BEC crossover theory to high temperature superconductors and ultracold atomic Fermi gases, *Low Temp. Phys.*, 2006, 32(4): 406; *Fiz. Nizk. Temp.*, 2006, 32: 538

58. S. Giorgini, L. P. Pitaevskii, and S. Stringari, Theory of ultracold atomic Fermi gases, *Rev. Mod. Phys.*, 2008, 80(4): 1215

59. C. Chin, R. Grimm, P. Julienne, and E. Tiesinga, Feshbach resonances in ultracold gases, *Rev. Mod. Phys.*, 2010, 82(2): 1225

60. M. Inguscio, W. Ketterle, and C. Salomon (Eds.), Ultracold Fermi gases, Proceedings of the International School of Physics "Enrico Fermi", Vol. CLXIV, Varenna, 2006, Società Italiana di Fisca Bologna, Italy (ISO press, Amsterdam, 2008)

61. H. Ding, T. Yokoya, J. C. Campuzano, T. Takahashi, M. Randeria, M. R. Norman, T. Mochiku, K. Hadowaki, and J. Giapintzakis, Spectroscopic evidence for a pseudogap in the normal state of underdoped high-T_c superconductors, *Nature*, 1996, 382(6586): 51

62. Ch. Renner, B. Revaz, K. Kadowaki, I. Maggio-Aprile, and O. Fischer, Observation of the low temperature pseudogap in the vortex cores of $Bi_2Sr_2CaCu_2O_{8+\delta}$, *Phys. Rev. Lett.*, 1998, 80(16): 3606

63. Ch. Renner, B. Revaz, J. Y. Genoud, K. Kadowaki, and O. Fischer, Pseudogap precursor of the superconducting gap in under- and overdoped $Bi_2Sr_2CaCu_2O_{8+\delta}$, *Phys. Rev. Lett.*, 1998, 80(1): 149

64. V. M. Krasnov, A. Yurgens, D. Winkler, P. Delsing, and T. Claeson, Evidence for coexistence of the superconducting gap and the pseudogap in Bi-2212 from intrinsic tunneling spectroscopy, *Phys. Rev. Lett.*, 2000, 84: 5860

65. M. Kugler, O. Fischer, Ch. Renner, S. Ono, and Y. Ando, Scanning tunneling spectroscopy of $Bi_2Sr_2CuO_{6+\delta}$: New evidence for the common origin of the pseudogap and superconductivity, *Phys. Rev. Lett.*, 2001, 86(21): 4911

66. J. W. Loram, K. Mirza, J. Cooper, W. Liang, and J. Wade, Electronic specific heat of $YBa_2Cu_3O_{6+x}$ from 1.8 to 300 K, *J. Superondutivity*, 1994, 7(1): 243

67. G. V. M. Williams, E. M. Haines, and J. L. Tallon, Pair breaking in the presence of a normal-state pseudogap in high-T_c cuprates, *Phys. Rev. B*, 1998, 57: 146

68. D. Walker, A. P. Mackenzie, and J. R. Cooper, Transport properties of zinc-doped $YBa_2Cu_3O_{7-\delta}$ thin films, *Phys. Rev. B*, 1995, 51: 15653(R)

69. T. Graf, J. M. Lawrene, M. F. Hundley, J. D. Thompson, A. Lacerda, E. Haanappel, M. S. Torikahili, Z. Fisk, and P. C. Canfield, Resistivity, magnetization, and specific heat of $YbAgCu_4$ in high magnetic fields, *Phys. Rev. B*, 1995, 51: 15053

70. Y. F. Yan, P. Matl, J. M. Harris, and N. P. Ong, Negative magnetoresistance in the *c*-axis resistivity of $Bi_2Sr_2CaCu_2O_{8+\delta}$ and $YBa_2Cu_3O_{6+x}$, *Phys. Rev. B*, 1995, 52: R751(R)

71. G. Williams, J. L. Tallon, R. Dupree, and R. Michalak, Transport and NMR studies of the effect of Ni substitution on superconductivity and the normal-state pseudogap in $YBa_2Cu_4O_8$, *Phys. Rev. B*, 1996, 54: 9532

72. G. Williams, J. L. Tallon, E. M. Haines, R. Michalak, and R. Dupree, NMR evidence for a d-wave normal-state pseudogap, *Phys. Rev. Lett.*, 1997, 78: 721

73. K. Magishi, Y. Kituoka, G.-Q. Zheng, K. Asayama, T. Kondo, Y. Shimakawa, T. Manako, and Y. Kubo, Spin-gap behavior in underdoped $TlSr_2(Lu_{0.7}Ca_{0.3})Cu_2O_y$: ^{63}Cu and ^{205}Tl NMR studies, *Phys. Rev. B*, 1996, 54: 3070

74. A. Goto, H. Yasuoka, K. Otzschi, and Y. Ueda, Phase diagram for the spin pseudogap in $LaBa_2Cu_3O_y$ studied by NMR, *Phys. Rev. B*, 1997, 55: 12736

75. J. Bobroff, H. Alloul, P. Mendels, V. Viallet, J.-F. Marucco, and D. Colson, ^{17}O NMR evidence for a pseudogap in the monolayer $HgBa_2CuO_{4+\delta}$, *Phys. Rev. Lett.*, 1997, 78: 3757

76. K. Ishida, K. Yoshida, T. Mito, Y. Tokumaga, Y. Kitaoka, K. Asayama, Y. Nakayama, J. Shimoyama, and K. Kishio, Pseudogap behavior in single-crystal $Bi_2Sr_2CaCu_2O_{8+\delta}$ probed by Cu NMR, *Phys. Rev. B*, 1998, 58: R5960(R)

77. A. V. Puchkov, D. N. Basov, and T. Timusk, The pseudogap state in high-T_c superconductors: An infrared study, *J. Phys.: Condens. Matter*, 1996, 8(48): 10049

78. D. N. Basov, R. Liang, B. Dabrowski, D. A. Bonn, W. N. Hardy, and T. Timusk, Pseudogap and charge dynamics in CuO_2 planes in YBCO, *Phys. Rev. Lett.*, 1996, 77: 4090

79. D. Basov, C. Homes, E. Singley, M. Strongin, T. Timusk,G. Blumberg, and D. van der Marel, Unconventional energetics of the pseudogap state and superconducting state in high-T_c cuprates, *Phys. Rev. B*, 2001, 63: 134514

80. J. M. Tranquada, P. M. Gehring, G. Shirane, S. Shamoto, and M. Sato, Neutron-scattering study of the dynamical spin susceptibility in $YBa_2Cu_3O_{6.6}$, *Phys. Rev. B*, 1992, 46: 5561

81. P. C. Dai, H. A. Mook, S. M. Hayden, and F. Dogan, Resonance as a measure of pairing correlations in the high-T_c superconductor $YBa_2Cu_3O_{6.6}$, *Nature*, 2000, 406: 965

82. B. Lake, G. Aeppli, T. E. Mason, A. Schroeder, D. F. McMorrow, K. Lefmann, M. Isshiki, M. Nohara, H. Takagi, and S. M. Hayden, Spin gap and magnetic coherence in a clean high-temperature superconductor, *Nature*, 1999, 400: 43

83. G. Ruani and P. Ricci, Transitions at $T > T_c$ in underdoped crystals of $YBa_2Cu_3O_{7-x}$ observed by resonant Raman scattering, *Phys. Rev. B*, 1997, 55: 93

84. X. K. Chen, J. G. Nacini, K. C. Hewitt, J. C. Irwin, R. Liang, and W. N. Hardy, Electronic Raman scattering in underdoped $YBa_2Cu_3O_{6.5}$, *Phys. Rev. B*, 1997, 56: R513(R)

85. R. Nemetschek, M. Opel, C. Hoffmann, P. F. Muller, R. Hackl, H. Berger, L. Forro, A. Er, and E. Walker, Pseudogap and superconducting gap in the electronic Raman spectra of underdoped cuprates, *Phys. Rev. Lett.*, 1997, 78: 4837

86. J. W. Quilty, H. J. Trodahl, and D. M. Pooke, Electronic Raman scattering from $Bi_2Sr_2CaCu_2O_{8+\delta}$: Doping dependence of the pseudogap and anomalous 600 cm^{-1} peak, *Phys. Rev. B*, 1998, 57: R11097

87. Z. A. Xu, N. Ong, Y. Want, T. Kakeshita, and S. Uchida, Vortex-like excitations and the onset of superconducting

phase fluctuation in underdoped $La_{2-x}Sr_xCuO_4$, *Nature*, 2000, 406: 486

88. Y. Wang, Z. A. Xu, T. Kakeshita, S. Uchida, and N. P. Ong, Onset of the vortexlike Nernst signal above T_c in $La_{2-x}Sr_xCuO_4$ and $Bi_2Sr_{2-y}La_yCuO_6$, *Phys. Rev. B*, 2001, 64: 224519
89. Y. Y. Wang, N. P. Ong, Z. A. Xu, T. Kakeshita, S. Uchida, D. Bonn, R. Liang, and W. Hardy, High field phase diagram of cuprates derived from the Nernst effect, *Phys. Rev. Lett.*, 2002, 88: 257003
90. S. Tan and K. Levin, Nernst effect and anomalous transport in cuprates: A preformed-pair alternative to the vortex scenario, *Phys. Rev. B*, 2004, 69(6): 064510
91. A. G. Loeser, Z. X. Shen, D. S. Dessau, D. S. Marshall, C. H. Park, P. Fournier, and A. Kapitulnik, Excitation gap in the normal state of underdoped $Bi_2Sr_2CaCu_2O_{8+\delta}$, *Science*, 1996, 273(5273): 325
92. A. Kanigel, U. Chatterjee, M. Randeria, M. R. Norman, G. Koren, K. Kadowaki, and J. C. Campuzano, Evidence for pairing above the transition temperature of cuprate superconductors from the electronic dispersion in the pseudogap phase, *Phys. Rev. Lett.*, 2008, 101(13): 137002
93. For simplicity, here we do not discuss electron doping, which is rather similar. Further information can be found in Ref. [7].
94. S. Chakravarty, R. B. Laughlin, D. K. Morr, and C. Nayak, Hidden order in the cuprates, *Phys. Rev. B*, 2001, 63(9): 094503
95. P. A. Lee, High T_c superconductors as doped Mott insulators: Fluctuating current and spin chirality, *Physica C*, 2000, 341–348: 63
96. P. A. Lee and X.-G. Wen, Vortex structure in underdoped cuprates, *Phys. Rev. B*, 2001, 63(22): 224517
97. C. Honerkamp and P. A. Lee, Staggered flux fluctuations and the quasiparticle scattering rate in the $SU(2)$ gauge theory of the t–J model, *Phys. Rev. Lett.*, 2003, 90(24): 246402
98. C. M. Varma, Non-Fermi-liquid states and pairing instability of a general model of copper oxide metals, *Phys. Rev. B*, 1997, 55(21): 14554
99. C. M. Varma, Theory of the pseudogap state of the cuprates, *Phys. Rev. B*, 2006, 73(15): 155113
100. J. W. Loram, K. A. Mirza, J. R. Cooper, and J. L. Tallon, Specific heat evidence on the normal state pseudogap, *J. Phys. Chem. Solids*, 1998, 59(10–12): 2091
101. J. L. Tallon and J. W. Loram, The doping dependence of T^* – What is the real high-T_c phase diagram? *Physica C*, 2001, 349(1–2): 53
102. Q. J. Chen, K. Levin, and I. Kosztin, Superconducting phase coherence in the presence of a pseudogap: Relation to specific heat, tunneling, and vortex core spectroscopies, *Phys. Rev. B*, 2001, 63(18): 184519
103. P. W. Anderson, The resonating valence bond state in La_2CuO_4 and superconductivity, *Science*, 1987, 235(4793): 1196
104. P. W. Anderson, P. A. Lee, M. Randeria, T. M. Rie, N. Trivedi, and F. C. Zhang, The physics behind high-temperature superconducting cuprates: The "plain vanilla" version of RVB, *J. Phys.: Condens. Matter*, 2004, 16(24): R755
105. N. Nagaosa and P. A. Lee, Ginzburg–Landau theory of the spin-charge-separated system, *Phys. Rev. B*, 1992, 45: 966
106. For a review of spin-harge separation, see: P. A. Lee, Pseudogaps in underdoped cuprates, *Physica C*, 1999, 317–318: 194
107. Y. J. Uemura, G. M. Luke, B. J. Sternlieb, J. H. Brewer, J. F. Carolan, et al., Universal Correlations between T_c and n_s/m^* (carrier density over effective mass) in high-T_c cuprate superconductors, *Phys. Rev. Lett.*, 1989, 62: 2317
108. Y. J. Uemura, Bose–Einstein to BCS crossover picture for high-T_c cuprates, *Physica C*, 1997, 282–287: 194
109. V. Mishra, U. Chatterjee, J. C. Campuzano, and M. R. Norman, Effect of the pseudogap on the transition temperature in the cuprates and implications for its origin, *Nat. Phys.*, 2014, 10(5): 357
110. V. J. Emery and S. A. Kivelson, Importance of phase fluctuations in superconductors with small superfluid density, *Nature*, 1995, 374: 434
111. M. Franz, Z. B. Tesanovic, and O. Vafek, QED3 theory of pairing pseudogap in cuprates: From d-wave superconductor to antiferromagnet via "algebraic" Fermi liquid, *Phys. Rev. B*, 2002, 66: 054535
112. I. Ussishkin, S. L. Sondhi, and D. A. Huse, Gaussian superconducting fluctuations, thermal transport, and the Nernst effect, *Phys. Rev. Lett.*, 2002, 89(28): 287001
113. J. N. Milstein, S. J. J. M. F. Kokkelmans, and M. J. Holland, Resonance theory of the crossover from Bardeen–Cooper-Schrieffer superfluidity to Bose–Einstein condensation in a dilute Fermi gas, *Phys. Rev. A*, 2002, 66(4): 043604
114. Y. Ohashi and A. Griffin, BCS–BEC crossover in a gas of Fermi atoms with a Feshbach resonance, *Phys. Rev. Lett.*, 2002, 89(13): 130402
115. N. Andrenacci, P. Pieri, and G. C. Strinati, Evolution from BCS superconductivity to Bose–Einstein condensation: Current correlation function in the broken-symmetry phase, *Phys. Rev. B*, 2003, 68: 144507
116. A. Perali, P. Pieri, L. Pisani, and G. C. Strinati, BCS–BEC crossover at finite temperature for superfluid trapped Fermi atoms, *Phys. Rev. Lett.*, 2004, 92(22): 220404
117. H. Hu, P. D. Drummond, and X. J. Liu, Universal thermodynamics of strongly interacting Fermi gases, *Nat. Phys.*, 2007, 3(7): 469
118. K. Levin, Q. J. Chen, Y. He, and C.-C. Chien, Comparison of different pairing fluctuation approaches to BCS–BEC crossover, *Ann. Phys.*, 2010, 325(2): 233
119. N. E. Bickers, D. J. Scalapino, and S. R. White, Conserving approximations for strongly correlated electron systems: Bethe–Salpeter equation and dynamics for the two-dimensional hubbard model, *Phys. Rev. Lett.*, 1989, 62: 961

120. N. E. Bickers and D. J. Scalapino, Conserving approximations for strongly fluctuating electron systems (I): Formalism and calculational approach, *Ann. Phys.*, 1989, 193: 206

121. R. Haussmann, W. Rantner, S. Cerrito, and W. Zwerger, Thermodynamics of the BCS–BEC crossover, *Phys. Rev. A*, 2007, 75(2): 023610

122. Y. O. R. Watanabe and S. Tsuchiya, Superfluid density of states and pseudogap phenomenon in the BCS–BEC crossover regime of a superfluid Fermi gas, *Phys. Rev. A*, 2010, 82: 043630

123. P. Magierski, G. Wlazöwski, A. Bulgac, and J. E. Drut, Finite-temperature pairing gap of a unitary Fermi gas by quantum Monte Carlo calculations, *Phys. Rev. Lett.*, 2009, 103(21): 210403

124. P. Pieri, A. Perali, G. C. Strinati, S. Riedl, M. J. Wright, A. Altmeyer, C. Kohstall, E. R. S. Guajardo, J. H. Denschlag, and R. Grimm, Pairing-gap, pseudogap, and no-gap phases in the radio-frequency spectra of a trapped unitary ^{6}Li gas, *Phys. Rev. A*, 2011, 84: 011608(R)

125. L. P. Kadanoff and P. C. Martin, Theory of many-particle systems (II): Superconductivity, *Phys. Rev.*, 1961, 124(3): 670

126. J. Stajic, J. N. Milstein, Q. J. Chen, M. L. Chiofalo, M. J. Holland, and K. Levin, Nature of superfluidity in ultracold Fermi gases near Feshbach resonances, *Phys. Rev. A*, 2004, 69(6): 063610

127. While a general interaction $V(\boldsymbol{k}-\boldsymbol{k}')$ may not be separable, it can however be de composed into different channels as $V(\boldsymbol{k}-\boldsymbol{k}')=\Sigma_l\varphi^l_{\boldsymbol{k}}\varphi^l_{\boldsymbol{k}'}$, where $\varphi^l_{\boldsymbol{k}}$ represents s-, p-, d-wave channels, etc. In most cases, only one channel dominates the superfluid order so that we may neglect other channels. In this way, the use of a separable potential is justified.

128. S. J. J. M. F. Kokkelmans, J. N. Milstein, M. L. Chiofalo, R. Walser, and M. J. Holland, Resonance superfluidity: Renormalization of resonance scattering theory, *Phys. Rev. A*, 2002, 65(5): 053617

129. Here we will mainly discuss s-wave short range contact potential for atomic Fermi gases. At present, p-wave superfluids are not yet available experimentally in atomic Fermi gases.

130. H. Guo, C.-C. Chien, Q. J. Chen, Y. He, and K. Levin, Finite-temperature behavior of an interspecies fermionic superfluid with population imbalance, *Phys. Rev. A*, 2009, 80: 011601(R)

131. J. B. Wang, Y. M. Che, L. F. Zhang, and Q. J. Chen, Searching for the elusive exotic Fulde–Ferrell–Larkin–Ovchinnikov states in Fermi–Fermi mixtures of ultracold quantum gases, arXiv: 1404.5696, 2014

132. C.-C. Chien, Q. J. Chen, Y. He, and K. Levin, Intermediate-temperature superfluidity in an atomic Fermi gas with population imbalance, *Phys. Rev. Lett.*, 2006, 97(9): 090402

133. C.-C. Chien, Q. J. Chen, Y. He, and K. Levin, Superfluid phase diagrams of trapped Fermi gases with population imbalance, *Phys. Rev. Lett.*, 2007, 98(11): 110404

134. Q. J. Chen, Y. He, C.-C. Chien, and K. Levin, Theory of superfluids with population imbalance: Finite-temperature and BCS–BEC crossover effects, *Phys. Rev. B*, 2007, 75(1): 014521

135. J. B. Wang, H. Guo, and Q. J. Chen, Exotic phase separation and phase diagrams of a Fermi–Fermi mixture in a trap at finite temperature, *Phys. Rev. A*, 2013, 87: 041601(R)

136. K. M. O'Hara, S. L. Hemmer, M. E. Gehm, S. R. Granade, and J. E. Thomas, Observation of a strongly interacting degenerate Fermi gas of atoms, *Science*, 2002, 298(5601): 2179

137. T. Bourdel, L. Khaykovich, J. Cubizolles, J. Zhang, F. Chevy, M. Teichmann, L. Tarruell, S. J. Kokkelmans, and C. Salomon, Experimental study of the BEC–BCS crossover region in lithium 6, *Phys. Rev. Lett.*, 2004, 93(5): 050401

138. J. Carlson, S. Y. Chang, V. R. Pandharipande, and K. E. Schmidt, Superfluid Fermi gases with large scattering length, *Phys. Rev. Lett.*, 2003, 91(5): 050401

139. I. Kosztin, Q. J. Chen, Y.-J. Kao, and K. Levin, Pair excitations, collective modes, and gauge invariance in the BCS-Bose–Einstein crossover scenario, *Phys. Rev. B*, 2000, 61(17): 11662

140. Q. J. Chen, Y. He, C.-C. Chien, and K. Levin, Stability conditions and phase diagrams for two-component Fermi gases with population imbalance, *Phys. Rev. A*, 2006, 74(6): 063603

141. In fact, the parameter γ can be taken from experiment, as has been done in Ref. [102], where one can find more details.

142. P. Pieri, L. Pisani, and G. C. Strinati, BCS–BEC crossover at finite temperature in the broken-symmetry phase, *Phys. Rev. B*, 2004, 70(9): 094508

143. N. Fukushima, Y. Ohashi, E. Taylor, and A. Griffin, Superfluid density and condensate fraction in the BCS–BEC crossover regime at finite temperatures, *Phys. Rev. A*, 2007, 75(3): 033609

144. I. Kosztin and A. J. Leggett, Nonlocal effects on the magnetic penetration depth in d-wave superconductors, *Phys. Rev. Lett.*, 1997, 79(1): 135

145. S. Hufner, M. A. Hossain, A. Damaselli, and G. Sawatzky, Two gaps make a high-temperature superconductor? *Rep. Prog. Phys.*, 2008, 71(6): 062501

146. G. Baskaran, Z. Zou, and P. W. Anderson, The resonating valence bond state and high-T_c superconductivity — A mean field theory, *Solid State Commun.*, 1987, 63(11): 973

147. N. Miyakawa, J. Zasadzinski, L. Ozyuzer, P. Guptasarma, D. Hinks, C. Kendziora, and K. Gray, Predominantly superconducting origin of large energy gaps in underdoped $Bi_2Sr_2CaCu_2O_{8+\delta}$ from tunneling spectroscopy, *Phys. Rev. Lett.*, 1999, 83(5): 1018

148. T.-L. Ho, Universal thermodynamics of degenerate quantum gases in the unitarity limit, *Phys. Rev. Lett.*, 2004, 92(9): 090402

149. M. L. Chiofalo, S. J. J. M. F. Kokkelmans, J. N. Milstein, and M. J. Holland, Signatures of resonance superfluidity in a quantum Fermi gas, *Phys. Rev. Lett.*, 2002, 88(9): 090402

150. Note here that the definition for n_c and n_p differ from that in Ref. [156] by a factor of 2.

151. G. E. Astrakharchik, J. Boronat, J. Casulleras, and S. Giorgini, Momentum distribution and condensate fraction of a fermion gas in the BCS–BEC Crossover, *Phys. Rev. Lett.*, 2005, 95: 230405 (Their result seems to suggest a tendency of decrease in the condensate fraction with an increasing particle number used for simulation.)

152. The curves in Fig. 19 were calculated using a two-channel model. Nevertheless, for wide Feshbach resonances such as in ^{6}Li and ^{40}K, the closed-channel fraction is very small [191, 192] so that the quantitative difference in the entropy $s(r)$ between the two-channel and one-channel model is negligible.

153. Q. J. Chen, J. Stajic, and K. Levin, Thermodynamics of interacting fermions in atomic traps, *Phys. Rev. Lett.*, 2005, 95(26): 260405

154. Q. J. Chen, C. A. Regal, M. Greiner, D. S. Jin, and K. Levin, Understanding the superfluid phase diagram in trapped Fermi gases, *Phys. Rev. A*, 2006, 73: 041601(R)

155. Note that the experimental data cannot be measuring $N_c = N$ as shown in Fig. 18, since at $1/(k_F a) = -1, N_c = N$ is far below the experimental threshold of detection.

156. J. Stajic, Q. J. Chen, and K. Levin, Density profiles of strongly interacting trapped Fermi gases, *Phys. Rev. Lett.*, 2005, 94: 060401

157. While one may argue that the kink, if it exists, may be smoothed out by the $\int \mathrm{d}y\mathrm{d}z$ integration, we note that as of the time of this writing, no kink behavior has ever been reported in 3D density profiles obtained via an inverse Abel transformation of experimental data.

158. Q. J. Chen, C. A. Regal, D. S. Jin, and K. Levin, Finite-temperature momentum distribution of a trapped Fermi gas, *Phys. Rev. A*, 2006, 74: 011601(R)

159. Q. J. Chen, Y. He, C.-C. Chien, and K. Levin, Theory of radio frequency spectroscopy experiments in ultracold Fermi gases and their relation to photoemission in the cuprates, *Rep. Prog. Phys.*, 2009, 72(12): 122501

160. C. H. Shunk, Y. Shin, A. Schirotzek, M. W. Zwierlein, and W. Ketterle, Determination of the fermion pair size in a resonantly interacting superfluid, *Nature*, 2008, 454(7205): 739

161. C. H. Schunk, Y. Shin, A. Schirotzek, M. W. Zwierlein, and W. Ketterle, Pairing without superfluidity: The ground state of an imbalanced Fermi mixture, *Science*, 2007, 316(5826): 867

162. Z. Yu and G. Baym, Spin-correlation functions in ultracold paired atomic-fermion systems: Sum rules, self-consistent approximations, and mean fields, *Phys. Rev. A*, 2006, 73(6): 063601

163. G. Baym, C. J. Pethick, Z. H. Yu, and M. W. Zwierlein, Coherence and clock shifts in ultracold Fermi gases with resonant interactions, *Phys. Rev. Lett.*, 2007, 99(19): 190407

164. M. Punk and W. Zwerger, Theory of RF-spectroscopy of strongly interacting fermions, *Phys. Rev. Lett.*, 2007, 99(17): 170404

165. A. Perali, P. Pieri, and G. C. Strinati, Competition between final-state and pairing-gap effects in the radio-frequency spectra of ultracold Fermi atoms, *Phys. Rev. Lett.*, 2008, 100(1): 010402

166. S. Basu and E. J. Müller, Final-state effects in the radio frequency spectrum of strongly interacting fermions, *Phys. Rev. Lett.*, 2008, 101(6): 060405

167. Y. He, C. C. Chien, Q. J. Chen, and K. Levin, Temperature and final state effects in radio frequency spectroscopy experiments on atomic Fermi gases, *Phys. Rev. Lett.*, 2009, 102(2): 020402

168. M. J. H. Ku, A. T. Sommer, L. W. Cheuk, and M. W. Zwierlein, Revealing the superfluid lambda transition in the universal thermodynamics of a unitary Fermi gas, arXiv: 1110.3309, 2011

169. E. Burovski, N. Prokof'ev, B. Svistunov, and M. Troyer, Critical temperature and thermodynamics of attractive fermions at unitarity, *Phys. Rev. Lett.*, 2006, 96(16): 160402

170. E. Burovski, E. Kozik, N. Prokof'ev, B. Svistunov, and M. Troyer, Critical temperature curve in BEC–BCS crossover, *Phys. Rev. Lett.*, 2008, 101(9): 090402

171. O. Goulko and M. Wingate, Thermodynamics of balanced and slightly spin-imbalanced Fermi gases at unitarity, *Phys. Rev. A*, 2010, 82(5): 053621

172. J. Kinnunen, M. Rodríguez, and P. Törmä, Pairing gap and in-gap excitations in trapped fermionic superfluids, *Science*, 2004, 305(5687): 1131

173. Y. He, Q. J. Chen, and K. Levin, Radio-frequency spectroscopy and the pairing gap in trapped Fermi gases, *Phys. Rev. A*, 2005, 72: 011602(R)

174. P. Massignan, G. M. Bruun, and H. T. C. Stoof, Twin peaks in RF spectra of Fermi gases at unitarity, *Phys. Rev. A*, 2008, 77: 031601(R)

175. J. T. Stewart, J. P. Gaebler, and D. S. Jin, Using photoemission spectroscopy to probe a strongly interacting Fermi gas, *Nature*, 2008, 454(7205): 744

176. Q. J. Chen and K. Levin, Momentum resolved radio frequency spectroscopy in trapped fermi gases, *Phys. Rev. Lett.*, 2009, 102(19): 190402

177. D. S. Jin, Private communications; D.S. Jin, American Physical Society March Meeting Talk B8.00002, 2009, abstract available at http://meetings.aps.org/link/BAPS.2009.MAR.B8.2

178. J. P. Gaebler, J. T. Stewart, T. E. Drake, D. S. Jin, A. Perali, P. Pieri, and G. C. Strinati, Observation of pseudogap behaviour in a strongly interacting Fermi gas, *Nat. Phys.*, 2010, 6(8): 569

179. A. Perali, F. Palestini, P. Pieri, G. C. Strinati, J. T. Stewart, J. P. Gaebler, T. E. Drake, and D. S. Jin, Evolution of the normal state of a strongly interacting Fermi gas from a pseudogap phase to a molecular Bose gas, *Phys. Rev. Lett.*, 2011, 106(6): 060402

180. A. Perali, P. Pieri, G. C. Strinati, and C. Castellani, Pseudogap and spectral function from superconducting fluctuations to the bosonic limit, *Phys. Rev. B*, 2002, 66(2): 024510

181. P. Pieri, L. Pisani, and G. C. Strinati, Pairing fluctuation effects on the single-particle spectra for the superconducting state, *Phys. Rev. Lett.*, 2004, 92(11): 110401

182. Y. Shin, M. W. Zwierlein, C. H. Schunck, A. Schirotzek, and W. Ketterle, Observation of phase separation in a strongly interacting imbalanced Fermi gas, *Phys. Rev. Lett.*, 2006, 97(3): 030401

183. S. Nascimbène, N. Navon, K. Jiang, F. Chevy, and C. Salomon, Exploring the thermodynamics of a universal Fermi gas, *Nature*, 2010, 463(7284): 1057

184. S. Nascimbène, N. Navon, S. Pilati, F. Chevy, S. Giorgini, A. Georges, and C. Salomon, Fermi-liquid behavior of the normal phase of a strongly interacting gas of cold atoms, *Phys. Rev. Lett.*, 2011, 106(21): 215303

185. L. P. Gor'kov and T. K. Melik-Barkhudarov, Contribution to the theory of superfluidity in an imperfect fermi gas, *Sov. Phys. JETP*, 1961, 13: 1018

186. H. Heiselberg, C. J. Pethick, H. Smith, and L. Viverit, Influence of induced interactions on the superfluid transition in dilute Fermi gases, *Phys. Rev. Lett.*, 2000, 85(12): 2418

187. D. H. Kim, P. Törmä, and J.-P. Martikainen, Induced interactions for ultracold Fermi gases in optical lattices, *Phys. Rev. Lett.*, 2009, 102(24): 245301

188. J. P. Martikainen, J. J. Kinnunen, P. Törmä, and C. J. Pethick, Induced interactions and the superfluid transition temperature in a three-component Fermi gas, *Phys. Rev. Lett.*, 2009, 103(26): 260403

189. Z. Q. Yu, K. Huang, and L. Yin, Induced interaction in a Fermi gas with a BEC–BCS crossover, *Phys. Rev. A*, 2009, 79(5): 053636

190. Q. J. Chen, Effect of the particle-hole channel on BCS–Bose–Einstein condensation crossover in atomic Fermi gases, arXiv: 1109.2307, 2011

191. Q. J. Chen and K. Levin, Population of closed-channel molecules in trapped Fermi gases with broad Feshbach resonances, *Phys. Rev. Lett.*, 2005, 95(26): 260406

192. G. B. Partridge, K. E. Strecker, R. I. Kamar, M. W. Jack, and R. G. Hulet, Molecular probe of pairing in the BEC–BCS crossover, *Phys. Rev. Lett.*, 2005, 95(2): 020404

193. H. Guo, C.-C. Chien, and K. Levin, Establishing the presence of coherence in atomic Fermi superfluids: Spin-flip and spin-preserving Bragg scattering at finite temperatures, *Phys. Rev. Lett.*, 2010, 105(12): 120401

194. M. G. Lingham, K. Fenech, S. Hoinka, and C. J. Vale, Local observation of pair condensation in a Fermi gas at unitarity, *Phys. Rev. Lett.*, 2014, 112(10): 100404